Круглый стол

Обзор некоторых работ предоставленных на ICCF27

The 27th International Conference on Condensed Matter Nuclear Science

August 31 – September 4, 2026, Niagara Falls, Canada



ICCF-27. Canada **53 oral presentations**+ posters?????

**SSF YouTube ICCF-27 <== Link Solid State Fusion Website Anthropocene Institute Website

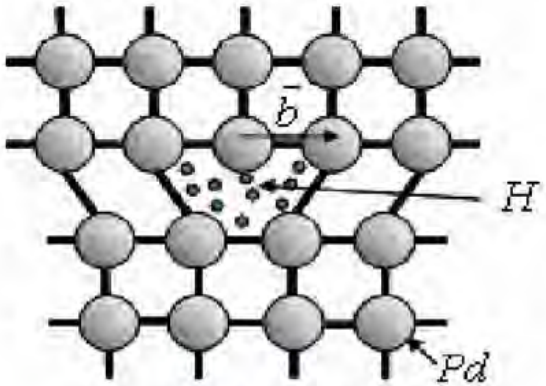

Aadhar RPBA Meijer - IWAHLM-16 - LENR: From Fusion Confusion to Paradigm Shift
24:47 / 25:37

Where Do LENR Occur?

David J. Nagel

Atoms in Dislocations and Grain Boundaries

H in Dislocations



https://www.lenr-canr.org/acrobat/MileyGHlenrreacti.pdf

Uniqueness of H Nuclei: 100,000 times smaller than atoms.

Diffusion of Titanium (dark) into Niobium (Light)



Fast diffusion along grain boundaries and slow diffusion into grains.

J. Grosso and D. J. Nagel. "Anodizing as a technique for studying diffusion in the TiNb system." AIME Met. Society Transactions, vol. 236.9, pp. 1377-1379 (1966)

Grain boundary segregation of impurities can impede normally-fast grain boundary diffusion.

Relationships between Some Defects in Materials

Grain boundaries, with their open structures, are like incipient gaps inside of lattices.

Super Abundant Vacancies might rearrange to form gaps or voids.

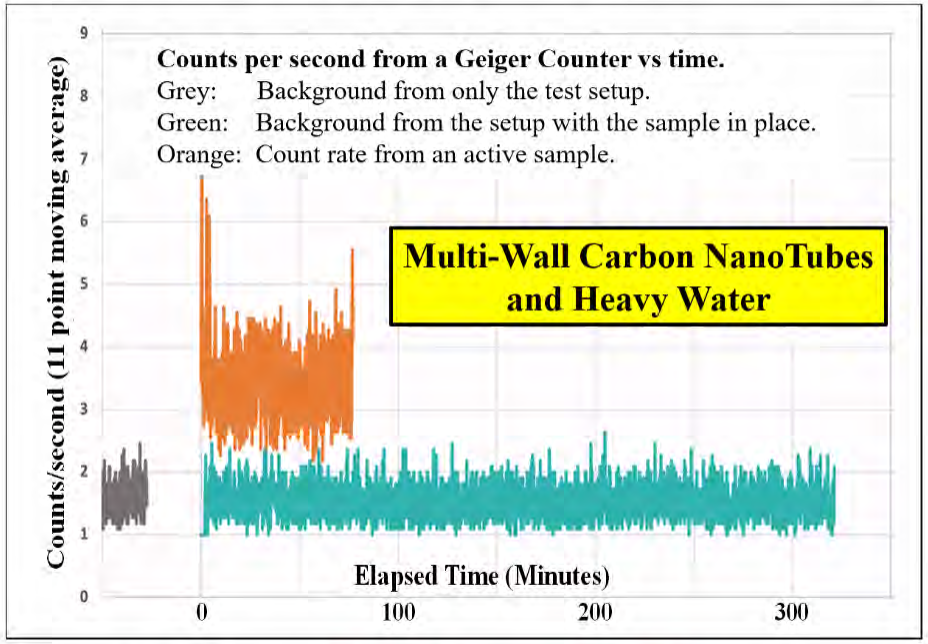
Gaps inside of materials are similar to pores between particles of powders.

Storms has proposed gaps within or between lattices, and distorted regions in lattices, as the locations where LENR occur:

The size of this distorted region is important. It needs to be small enough for the negative charge density from the nearby-distorted electrons to be large enough to reduce the positive charge on the D nuclei but larger than a normal atom vacancy. The required size is proposed to be in the 10 nm range.

E. Storms, This Conference

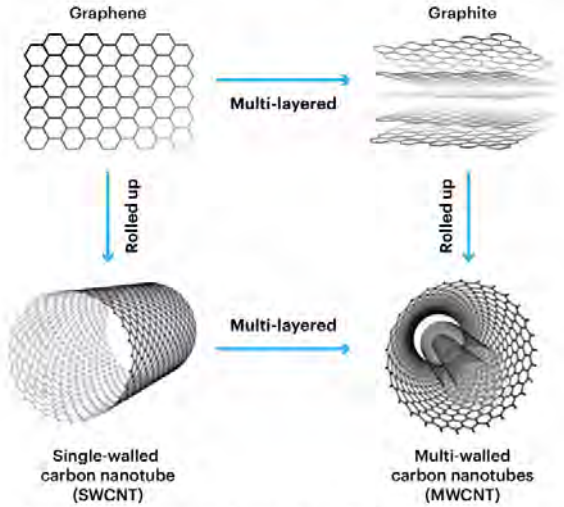
Evidence that Nano-Scale Structures Cause LENR



https://www.**deuteriumenergetics**.com/

Carbon NanoTubes

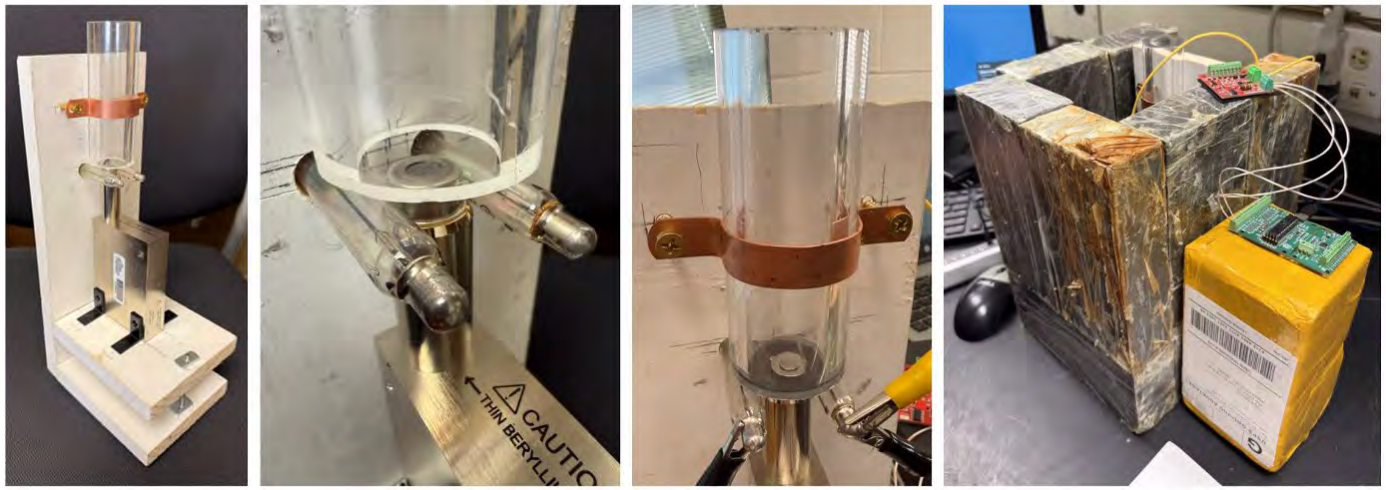
https://en.wikipedia.org/wiki/Carbon_nanotube



https://tuball.com/articles/single-walled-carbon-nanotubes

Current Replication Attempts at GWU

Emanuele F. Marano and David J. Nagel



https://www.**amptek**.com/products/x-ray-detectors/**cdte-x-ray-and-gamma-ray-detectors**

Three Remarkable Reports from LENR Experiments

1985 Fleischmann-Pons Meltdown.

M. Fleischmann, S. Pons, and M. Hawkins,
"Electrochemically induced nuclear fusion of deuterium."
J. Electroanalytical Chemistry, vol. 261, p. 301 (1989)

1996 Preparata Report:

CF power densities can reach the incredible values of 50-100 kW/cm^3

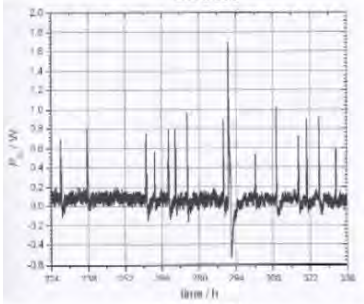
G. Preparata, "Everything Thing You Always Wanted to Know About Cold Fusion Calorimetry"
Progress in New Hydrogen Energy, Tokyo Institute of Technology, Tokyo (1996)

2006 Deuterium Energetics Discovery:

Carbon NanoTubes and Heavy Water Produce Hard Radiation
https://www.deuteriumenergetics.com/technology

WHEN do LENR Occur?

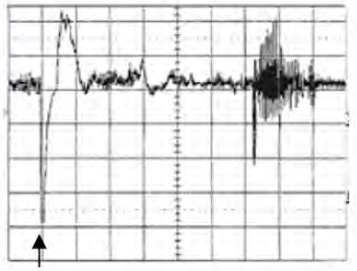
Heat



14 hr/div

H. Kozima, W.-S. Zhang and J. Dash, Precision measurement of excess energy in electrolytic system Pd/D/H_2SO_4 and inverse power distribution of energy pulses vs. excess energy, Proc. of the 13th Int. Conf. on CMNS, pp. 348–358 (2008)

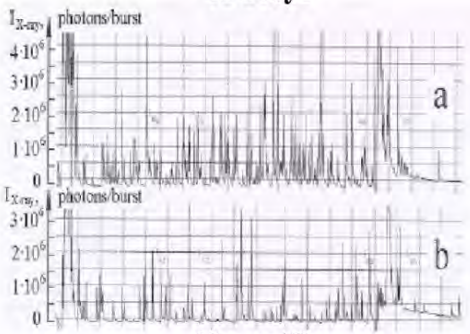
Sound



200 ms/div

S. Szpak, P.A. Mosier-Boss and F.E. Gordon, Experimental evidence for LENR in a Polarized Pd/D Lattice, presented at National Defense Industry Association Conference, Washington DC, 2006, and http://lenr-canr.org/wordpress/?page_id=1081

X-Rays



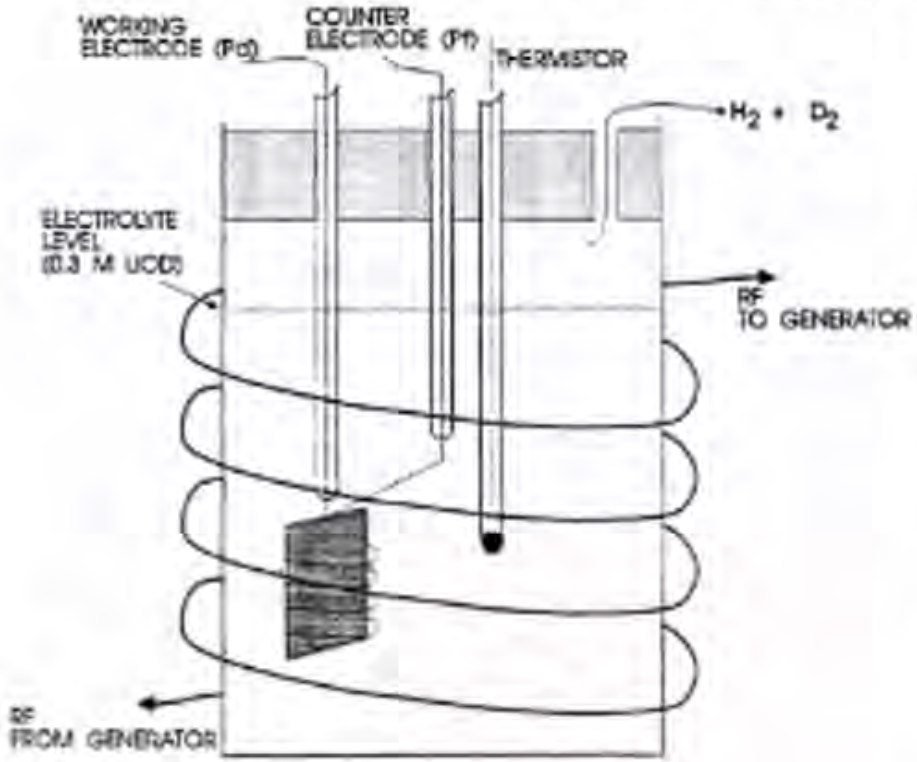
20 µsec/div

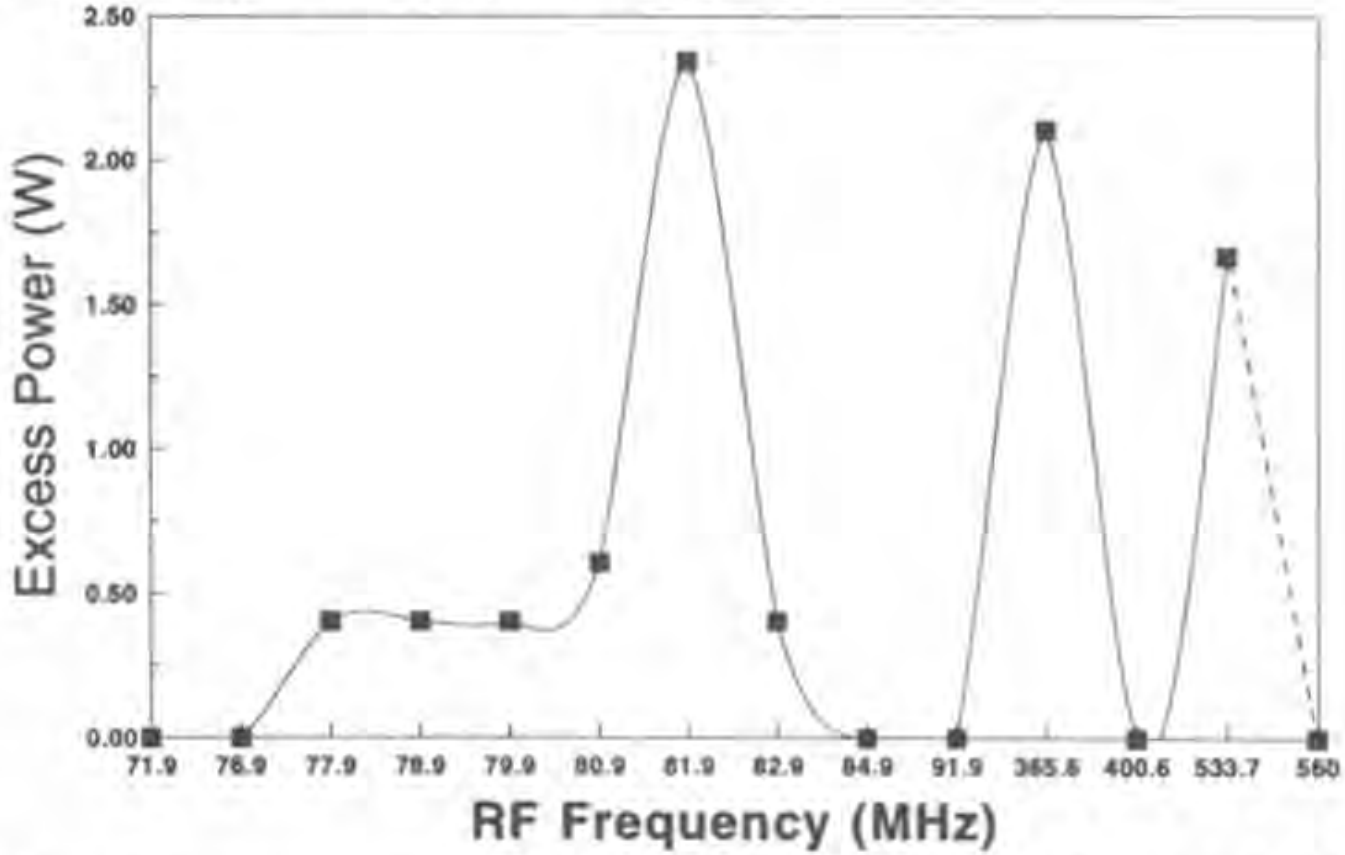
A.B. Karabut and S.A. Kolomeychenko, Experiments characterizing the X-ray emission from a solid-state cathode using a high-current glow discharge, Proc. 10th Int. Conf. on Condensed Matter Nuclear Science, World Scientific, Singapore, pp. 585–596 (2006)

Mathieu Valat *et al.*, "Observation of Heat Bursts during Electrolysis of Palladium in Heavy Water", This Conference

What is the Relationship between LENR Experiments and Radio Frequencies?

J. O'M. Bockris *et al.*, "Triggering of Heat and Sub-Surface Changes in Pd-D System," Transactions of Fusion Technology, vol. 26, pp. 267-290 (1994)





Felix Scholkmann , David J. Nagel and Louis F. DeChiaro, "Electromagnetic Emission in the kHz to GHz Range Associated with Heat Production During Electrochemical Loading of Deuterium into Palladium: A Summary and Analysis of Results Obtained by Different Research Groups", J. Condensed Matter Nuclear Science, vol. 19, pp. 325–335 (2016)

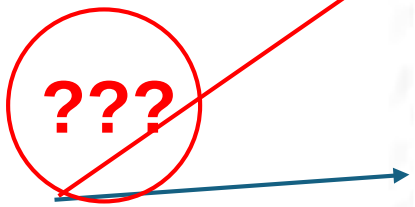
Commercialization

Two Main Challenges:

Scaling up to useful powers (> 1 kW)

Materials that work for extended periods.

LENR Companies:



AquaTerra Fusion	Thailand	https://aquaterrafusion.com/
Aureon Energy	Canada	https://www.aureonenergy.com/
Brillouin Energy	USA	https://brillouinenergy.com/
Clean Planet	Japan	https://www.cleanplanet.co.jp/
Deuterium Energetics	USA	https://www.deuteriumenergetics.com/
ENG8	Portugal	https://eng8.energy/
HYLENR	India	https://www.hylenr.com/
Leonardo	USA	https://ecatthenewfire.com/
Metatron NRG	Israel	https://metatron-nrg.com/
NHF-Energy Inc.	Japan	https://www.nhf-energy.com/
Prometheus	Italy	https://prometheusreactor.com/home/homepage
Solitonix	Italy	

Gamow-factor is replaced by $e^{-\frac{33.8}{T(MK)^{\frac{1}{3}}}}$ mann-factor due to resonance in L $e^{-\frac{E_0}{T(K)}}$

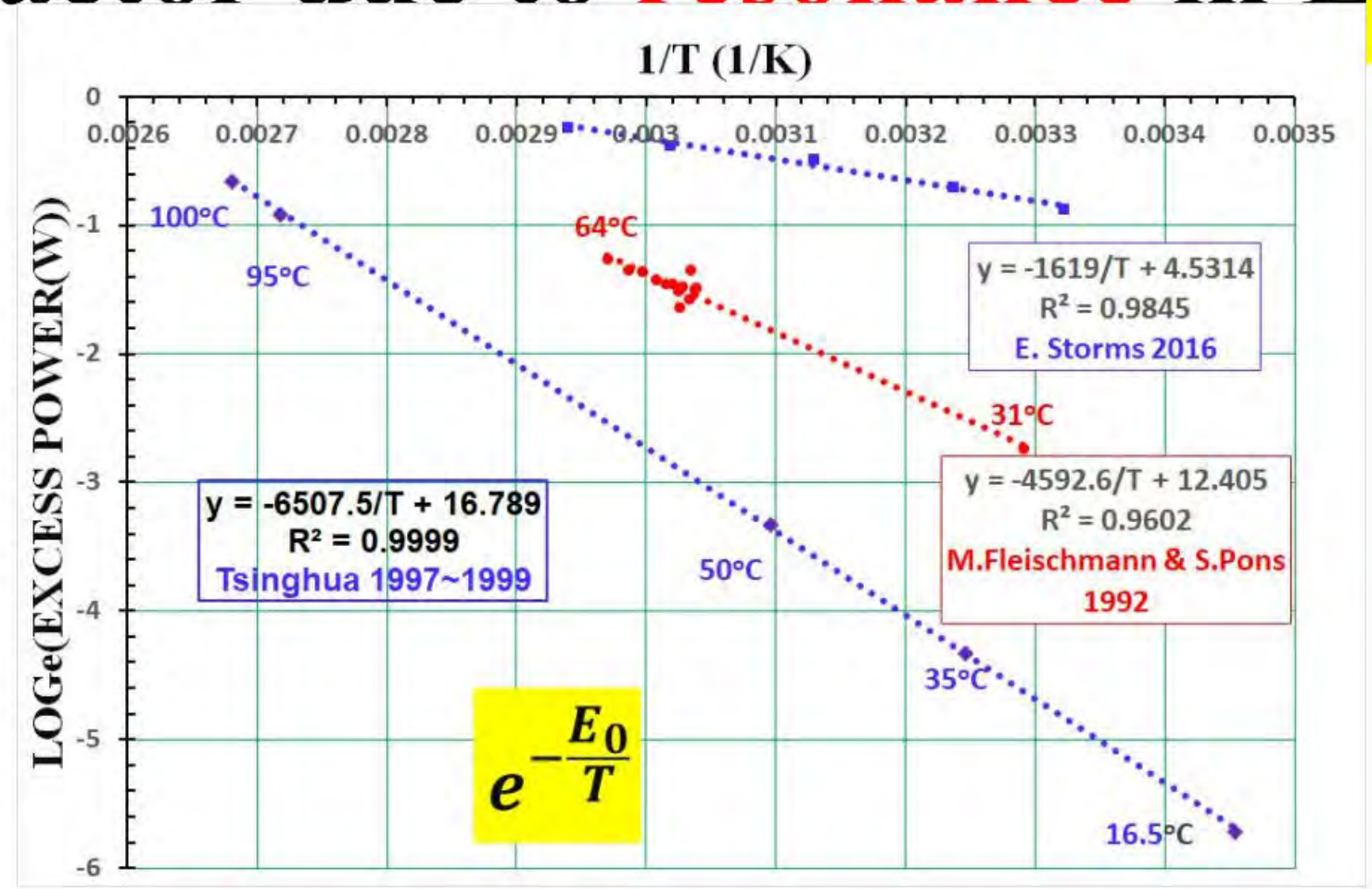


D. Nagel,

T. Passell,

G. Miley & M. Miles

J. Rothwell & F. Will



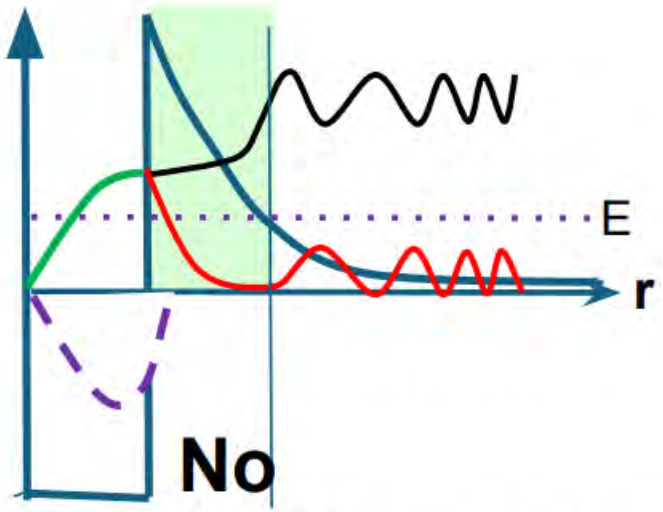
Tsinghua University, Beijing, CHINA

lxz-dmp@tsinghua.edu.cn

Huizenga 1989

Nuclear fusion at room temperature, ….would require the **invention of an entirely new nuclear process.**

$$e^{-\frac{33.8}{T(MK)^{\frac{1}{3}}}}$$



No Resonance

#1 Barrier

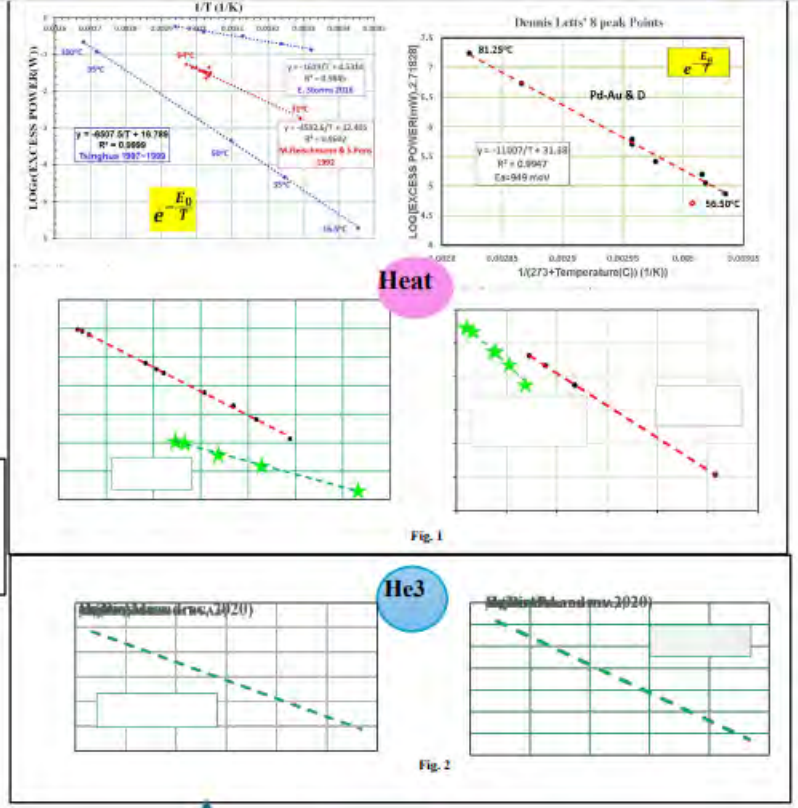
Bethe, 1938 Solar Energy

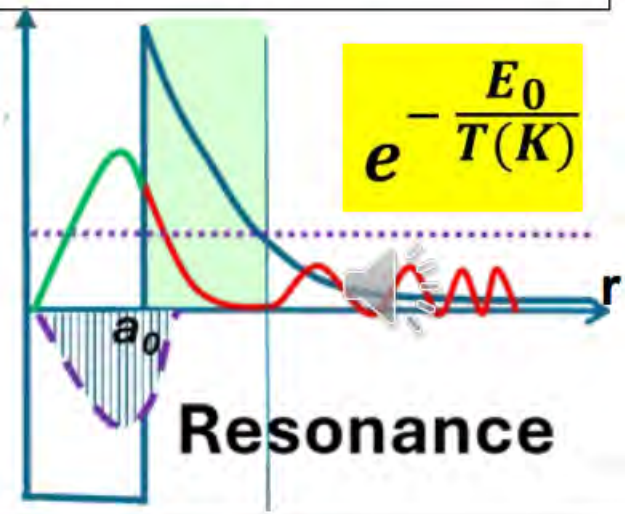
#2 Energy Transfer

Oppenheimer Stripping, 1935

#3 Radiation

Koonin's Formula, in "Nature",1989

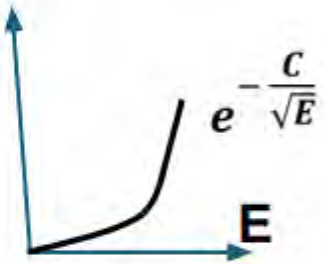


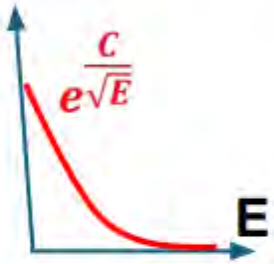


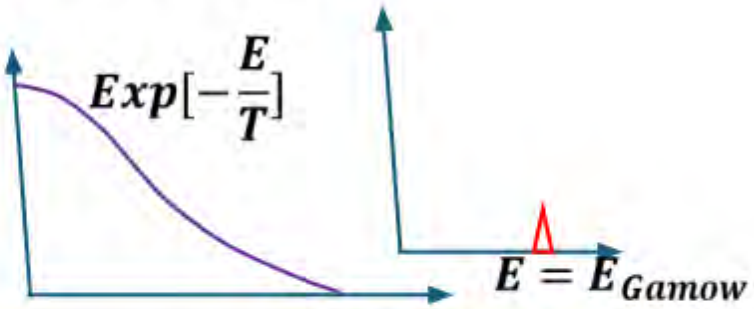
Resonance

Bethe's Model included both Gamow & Boltz

$$e^{-\frac{33.8}{T(MK)^{\frac{1}{3}}}}$$

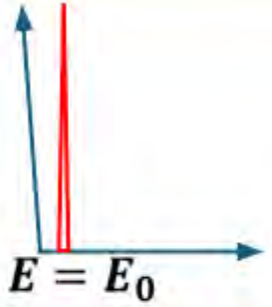




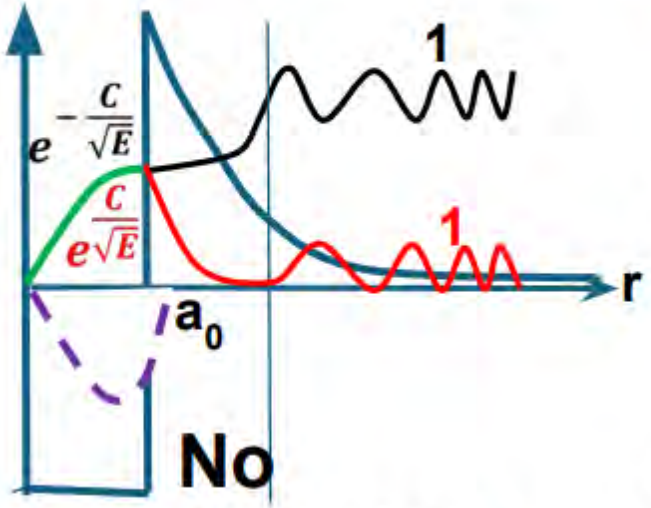


$$< \sigma v > \propto \int \left| \frac{Cot\delta}{\sqrt{1+(Cot\delta)^2}} F(a_0) + \frac{1}{\sqrt{1+(Cot\delta)^2}} G(a_0) \right|^2 Exp[-\frac{E}{T}]\, dE$$

$$Cot\delta \propto e^{\frac{2C}{\sqrt{E}}} \{[Log\phi]' - [LogG]'\}$$

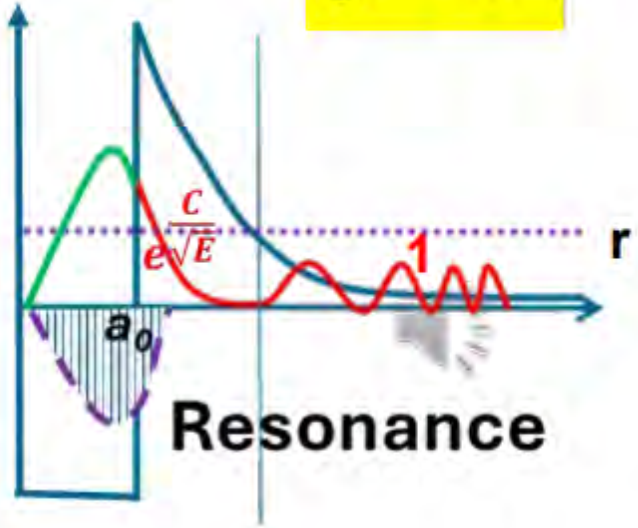


$$e^{-\frac{E_0}{T(K)}}$$



No Resonance

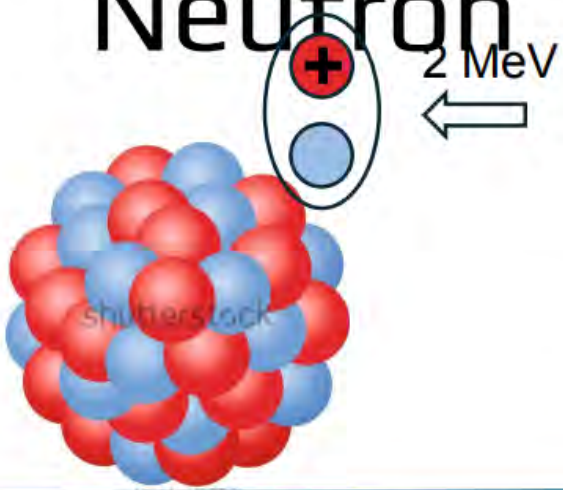
- Had Bethe lived to see Storms', he would have solved Puzzle #1 already.
- Z >1, d+Metal.



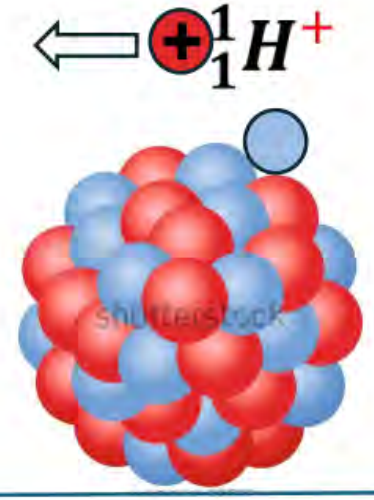
Resonance

Oppenheimer ---No Neutron

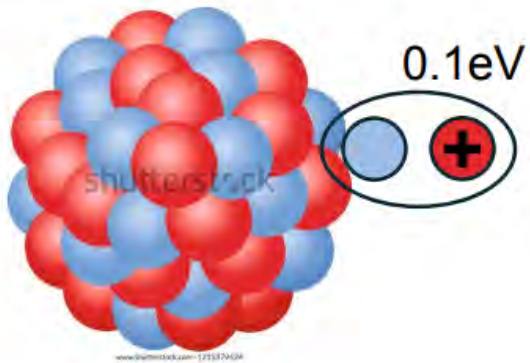
Strippin g



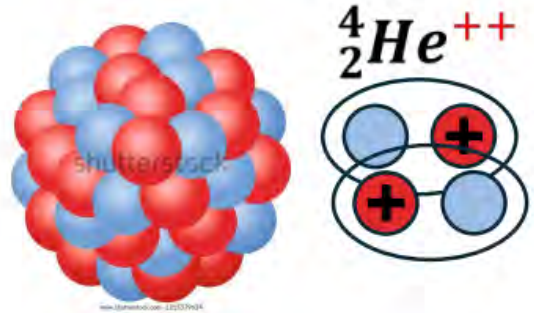
M(d,p)M’



Pick-U p

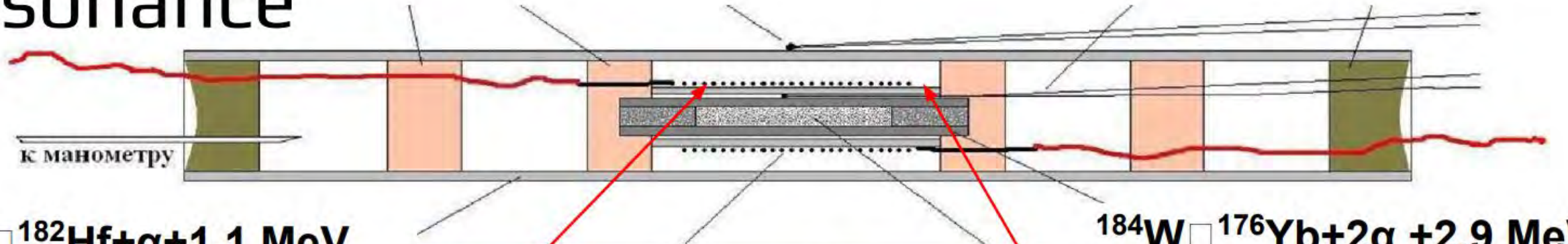


M(d, α)M”



- **Charged Particles ($^{4}_{2}He^{++}$, $^{1}_{1}H^{+}$) Transfer Nuclear Energy to Electrons**
- **Excess Heat without Neutron, Puzzle #2**

Ni-H, 1800°C, 1kW, 7 months—DoorWay Resonance



$^{186}W \square ^{182}Hf+\alpha+1.1$ MeV

$^{184}W \square ^{176}Yb+2\alpha$ +2.9 MeV



- W might be the fuel, rather than a heater only

Summary—3 Puzzles Solved with New Reaction

1. **Resonance is possibly the New Nuclear Process to solve 3 Puzzles.**
2. **Metal is burning with H(D) together, rather than burns d+d inside**





3. **Door Way Resonance induced α-emission is an important reaction**
4. **W is a favorable fuel for LENR**

BioTransmutation LENR Experiments: Review and Prospects

Amogha Gummadivalli[1], Ayan Marin[2] and David J. Nagel[3]

[1]Chantilly High School, Chantilly, Virginia, USA
[2] The Dalton School, New York, NY, USA
[3]George Washington University, Washington DC, USA

Articles on BioTransmutation LENR Experiments

There are a few dozen articles on BioTransmutation experiments.
The 2012 review by Biberian is a good way to learn about the topic:

J.-P. Biberian, "Biological Transmutations: Historical Perspective",
J. Condensed Matter Nuclear Science, vol 7. pp. 11–25 (2012)

In this review paper, it is shown that in biological systems, **chemical elements can be transmuted into other elements.** These facts have been established since the early 19th century, but they have been ignored by established science ever since. The purpose of this work is to show how during the past two centuries, a number of experimentalists have questioned the mass conservation law established by Antoine Lavoisier [1] for chemical reactions. They have proved experimentally in plants, bacteria and other living organisms, some elements are transmuted into other elements.

Reviews of BioTransmutation LENR Experiments

https://www.researchgate.net/profile/David-Cuthbertson-2/publication/265081345_A_Review_of_Research_on_the_Biological_Transmutation_of_Chemical_Elements/links/5ba4e32ca6fdccd3cb686779/A-Review-of-Research-on-the-Biological-Transmutation-of-Chemical-Elements.pdf (2007)

Kozima provided a review with two dozen pages in 2016.
J. Kozima, Proc. JCF16, 16-18, pp. 216–239 (2016), ISSN 2187-2260

The most recent review is by Biberian in 2020.
J.-P. Biberian, "Biological Transmutations", in J.-P. Biberian (Editor)
Cold Fusion: Advances in Condensed Matter Nuclear Science, Elsevier (2020)

Biology Can Transmutate the Elements

Desire' D. Dubounet (Editor) , Eclosion Kft. Budapest, Hungary, ISBN 978-615-5405-07-5
https://www.scribd.com/document/778655813/Biology-Can-Transmutate-the-Elements-pt-BR

Theory of BioTransmutations

There are a few dozen theories about LENR, but none of them are widely accepted, or satisfactorily compared with LENR experiments.

The most recent theoretical paper on BioTransmutations is from 2023:

Scientific Research Publishing

Journal of Modern Physics, 2023, 14, 1087-1116
https://www.scirp.org/journal/jmp
ISSN Online: 2153-120X
ISSN Print: 2153-1196

Explanation of Cold Nuclear Fusion and Biotransmutations

Auguste Meessen

UCLouvain, Louvain-la-Neuve, Belgium

Summary of Reactions Considered by Kervan (1960-1980)

$Na^{23} + H^{1} \rightarrow Mg^{24}$
$Na^{23} \rightarrow Li^{7} + O^{16}$
$Mg^{24} + O^{16} \rightarrow Ca^{40}$
$Cl^{35} \rightarrow C^{12} + Na^{23}$
$O^{16} + O^{16} \rightarrow S^{32}$
$Si^{28} + C^{12} \rightarrow Ca^{40}$

$Na^{23} + O^{16} \rightarrow K^{39}$
$K^{39} + H^{1} \rightarrow Ca^{40}$
$F^{19} + O^{16} \rightarrow Cl^{35}$
$Fe^{56} - H^{1} \rightarrow Mn^{55}$
$2\,N^{14} \rightarrow C^{12} + O^{16}$
$Si^{28} + C^{12} \rightarrow Ca^{40}$

$Na^{23} - O^{16} \rightarrow Li^{7}$
$Mg^{24} + Li^{7} \rightarrow P^{31}$
$C^{12} + Li^{7} \rightarrow F^{19}$
$2\,O^{16} - H^{1} \rightarrow P^{31}$
$N^{14} + Mg^{12} \rightarrow K^{19}$
$P^{31} + H^{1} \rightarrow S^{32}$

The considered reactions included both
reactions with protons and reactions between heavy elements.

Edmund Storms. A Comprehensive Explanation of the Cold Fusion Mechanism
Aug. 31 – Sept. 4, 2026 Niagara Falls, Canada
storms2@ix.netcom.com

- **What does it mean for the six abnormal phenomena observed in preliminary experiments of ^{17}O water ?**

(1) Lower NMR signals for high-concentration samples
(2) Lower MS signals for high-concentration samples
(3) Abnormal m/z 16 data in MS for gas sample from LENR
(4) Viscosity varies with ^{17}O concentration
(5) Conductivity of ^{17}O water increases in magnetic field
(6) Abnormal density curve

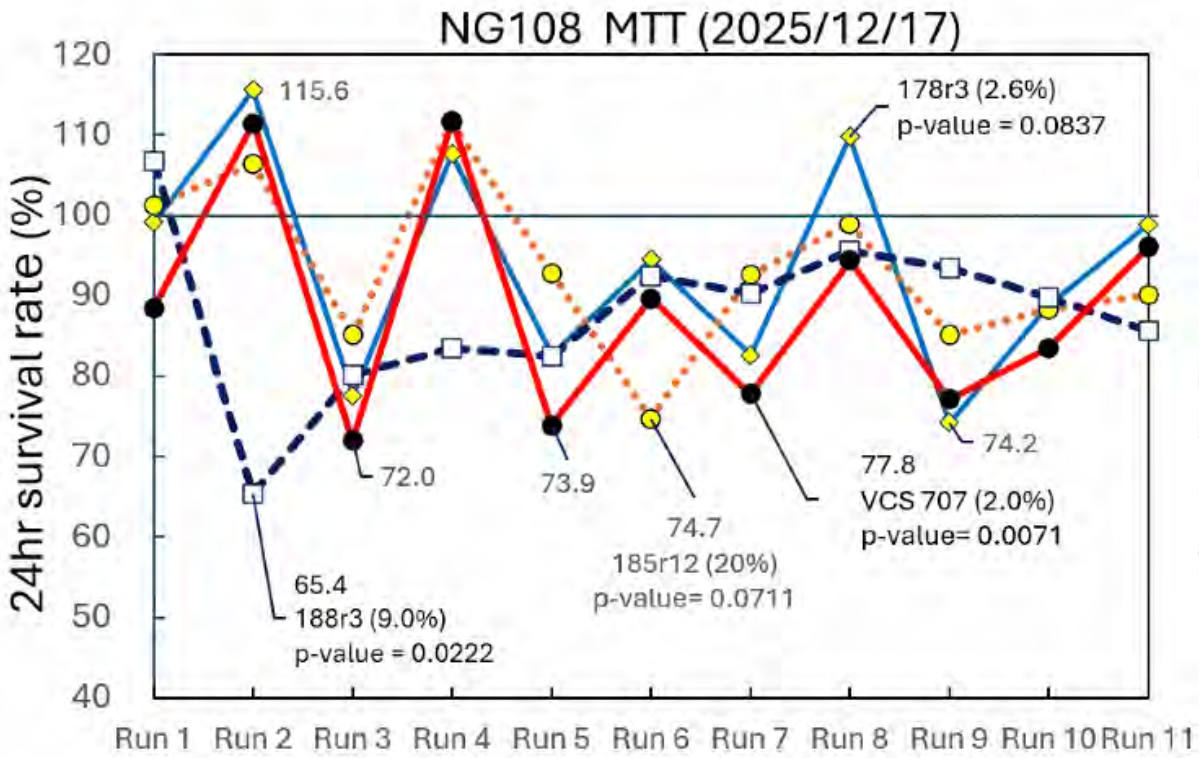
There must be some kind of quantum phenomenon producing these anomalous results ?

Further research is needed

5. MTT assays of cancer cells using ^{17}O-enriched water

(1) NG108 neuroblastoma cell line MTT assay results - 24h survival rate (S.R.)

- probability for S.R.(24h survival rate) < 100% with different ^{17}O-water: 73~91%
- overall probability for S.R. < 85%: 36% (total samples 44)



^{17}O water	Inhibition probability for 24h S.R.<100%
188r3	10/11 (91%)
VCS 707	9/11 (82%)
185r12	8/11 (73%)
178r3	8/11 (73%)

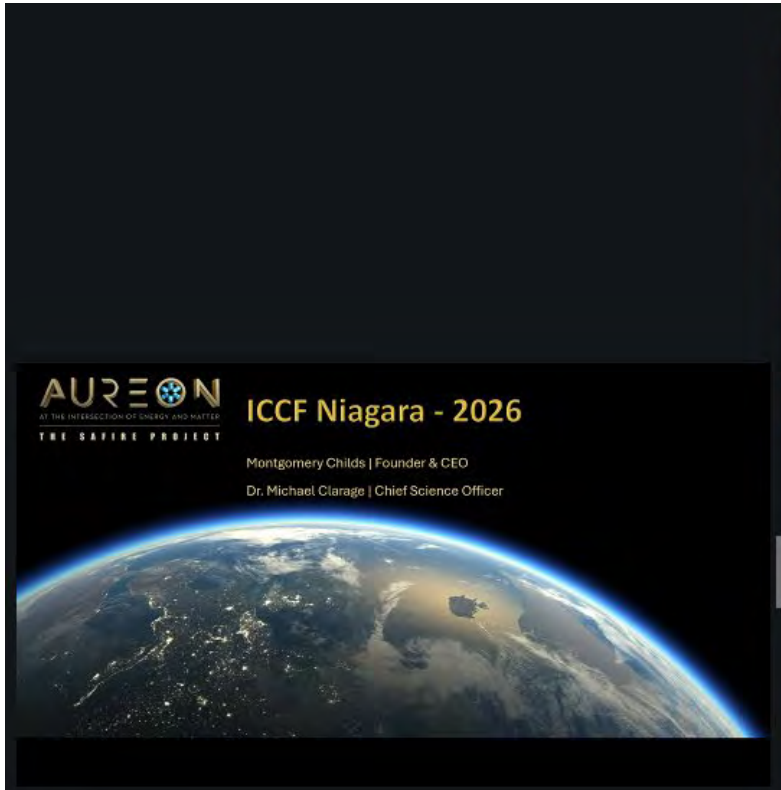
Survival rate (S.R.)	Overall probability
<80%	9/44= 20%
<85%	16/44= 36%

6. Conclusions

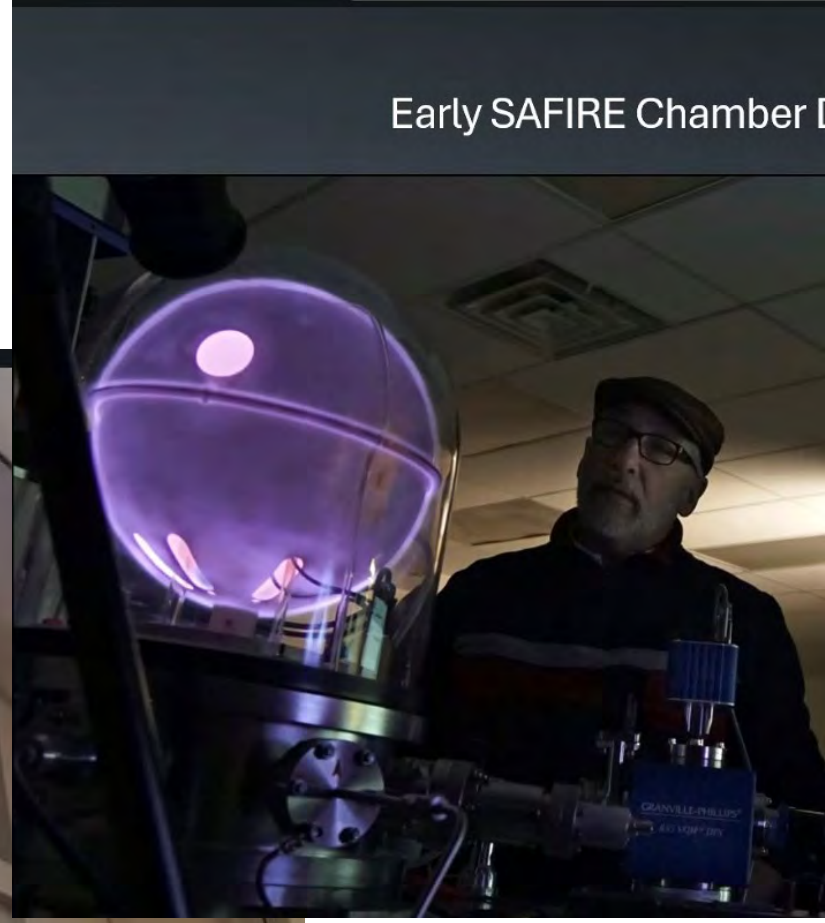
- DEX-1G produces 32 L batches assessed at ~30 mol% ^{17}O by our in-line dilution method; independent assay underway.
- Concentration measurement of ^{17}O-enriched water using NMR and MS by dilution method seems feasible. But still need third-party assay (underway).
- The LENR-treated water may become activated with some electromagnetic shielding effects interfering NMR and MS signals.
- If concentration data are correct, there seems a huge amount of concealed fusion energy stored as 'quantum latent heat' in plasmon of Quantum Coherent Lattice or in Microscopic Superconducting Current.
- MTT assays using ^{17}O-enriched water seems reveal that cancer cells metabolic activity may be interfered by MIE (Magnetic Isotope Effect) .
- Many of the anomalous behaviors observed in ^{17}O-enriched water may imply new physical mechanisms that warrant further investigation.

➢ Our conclusions are all based on experimental observations, from which we have speculated on the underlying physical mechanisms; further in-depth research by experts and academics is still required to confirm them.

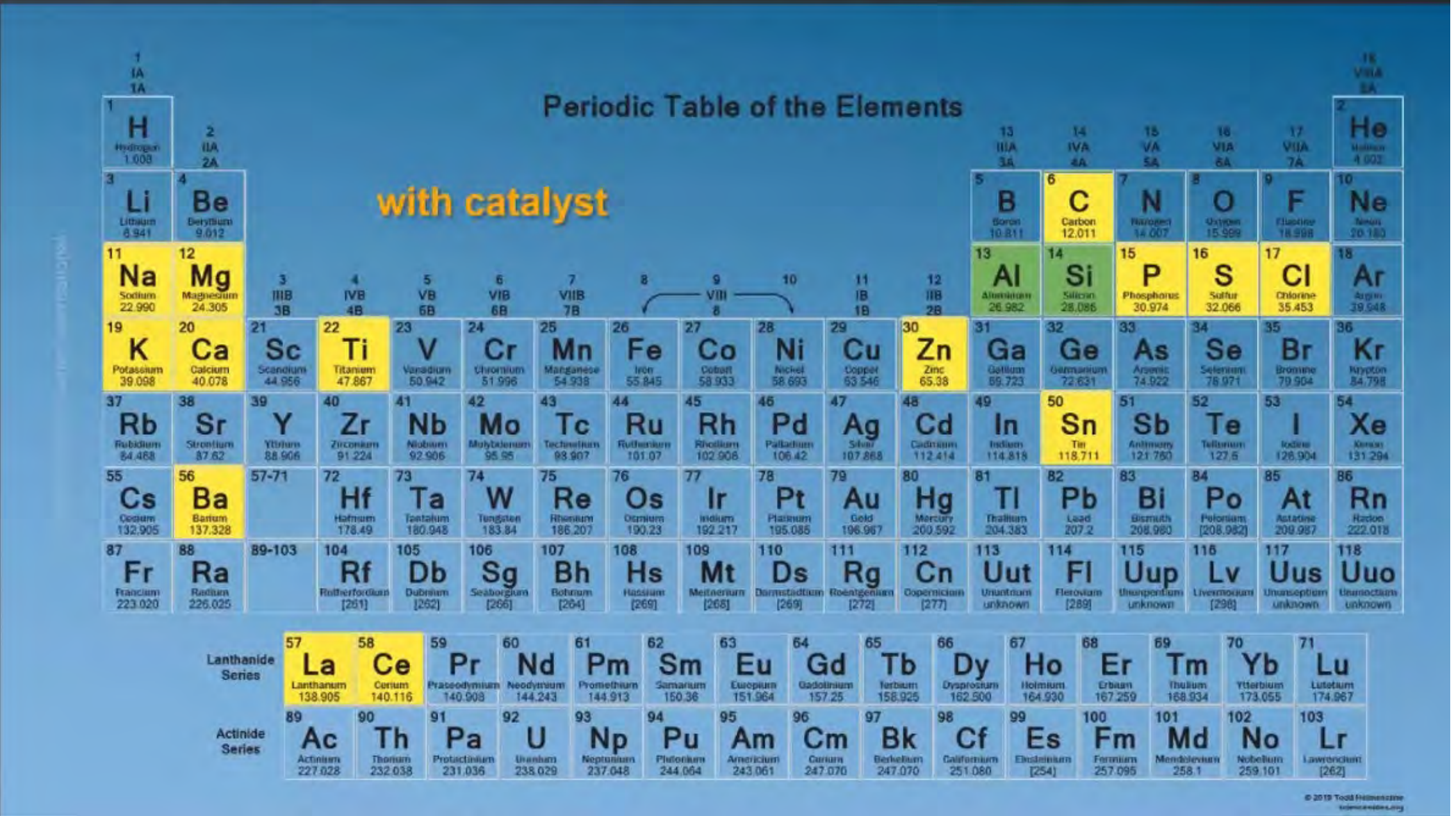
SAFIRE → AUREON, Canada



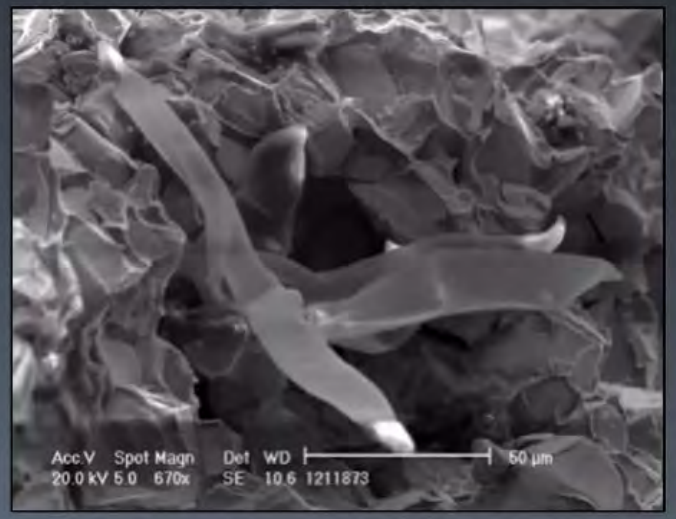


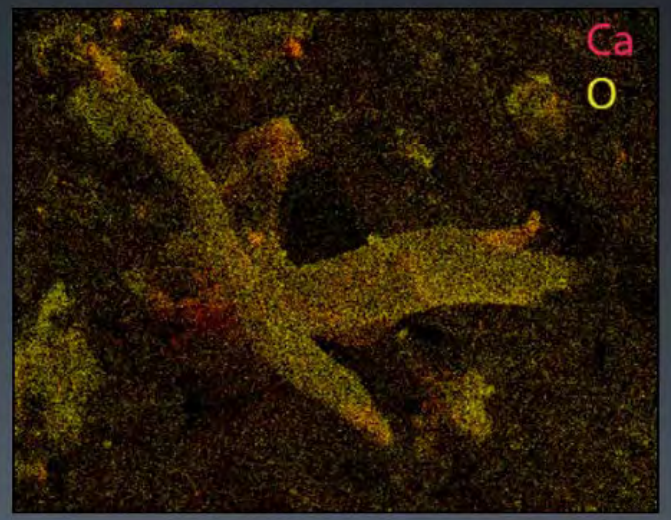


Elements produced in plasma chamber

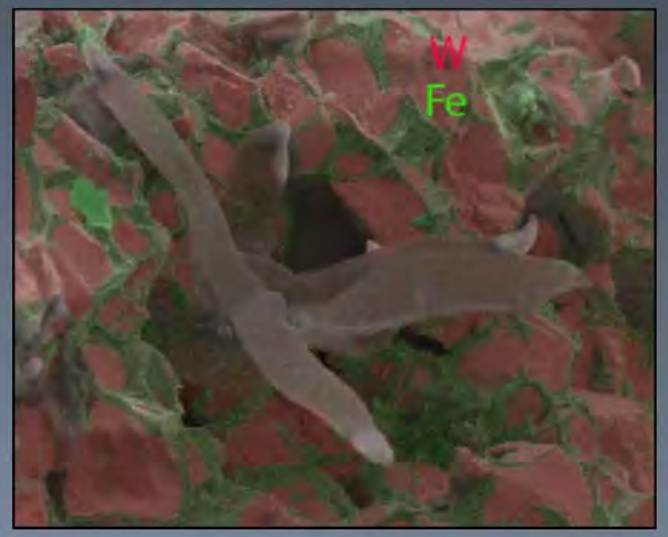


Calcium Ribbons in sintered Tungsten

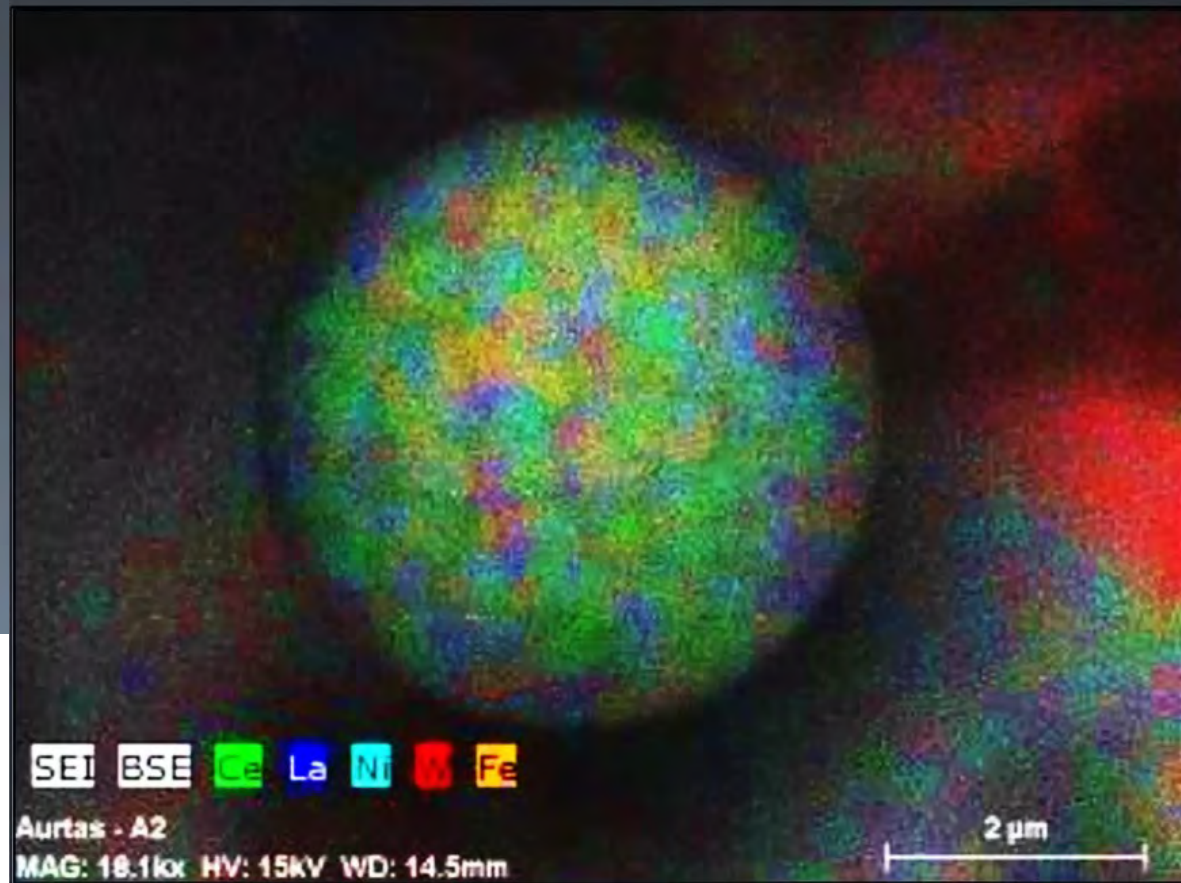




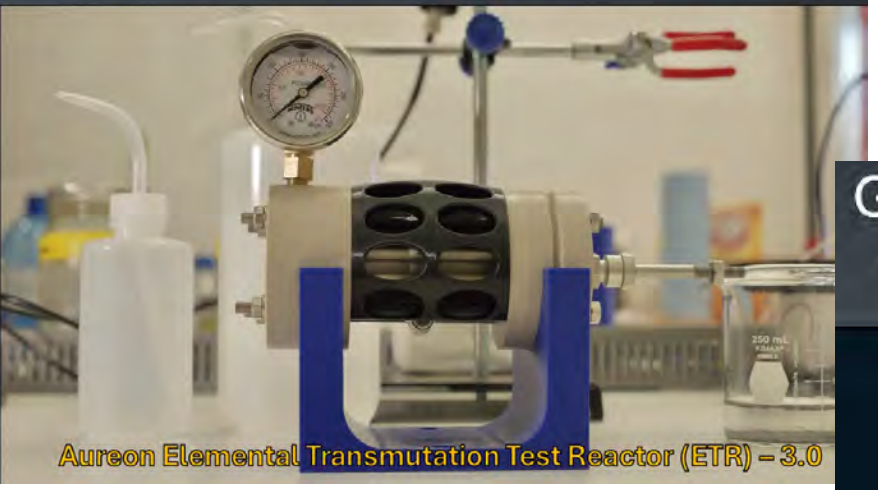




Common Ce, La, Ni, Fe sphere in W matrix



The Aureon ETR that Changed the Nucleus of Thorium
Remediation of Radioactive Waste / Fracking Water



Gel Laboratories USA – Third Party Validation – Control / Treated

ICP-MS measures, Blue= control, Green = from Thorium fuel.



Commercial viability - Two factors to consider:

Energy gain per reaction – COP
&
Reactions per second

Positive COP alone is not enough; you need a sufficient number of reactions per second for commercial viability.

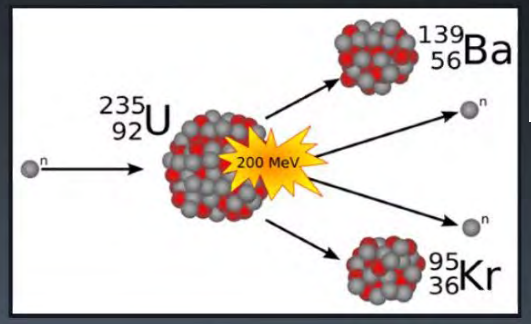
Summary Table for LENR Rates

From D. Nagel 2026 Bergamo presentation

Authors (Date)	Conditions	Rates (Hz)
Experimental LENR Rates		
Miley & Patterson (1996)	Film (Ni)	2×10^{11}
Dufour et al (1996)	Pd Wire	1.2×10^{7}
Iwamura et al (2002)	Surface (Pd)	4.7×10^{10}
Iwamura et al (2012)	Surface (Pd)	8.2×10^{10}
H. Takahashi et al (2012)	Surface (Pd)	$\sim 10^{6}$
Theoretical LENR Rates		
Y.E.Kim (1999 and 2012)	Bulk (BEC)	10^{14}
Widom & Larsen (2006)	Surface	10^{12}
Parkhomov (2015)	Bulk Ni, Al, Li	$10^{14} - 10^{15}$

Uranium fission has a huge COP.

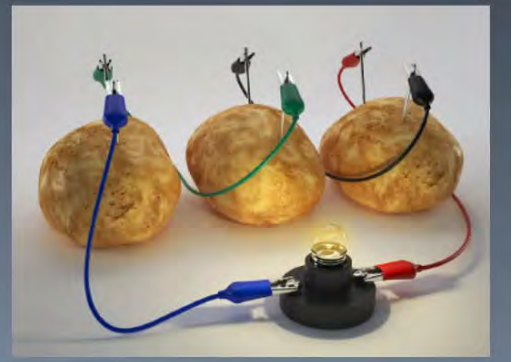
1eV neutron produces 200MeV of energy.



10^{19} reactions per second

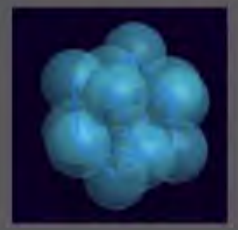


10^{10} reactions per second
1 watt LED

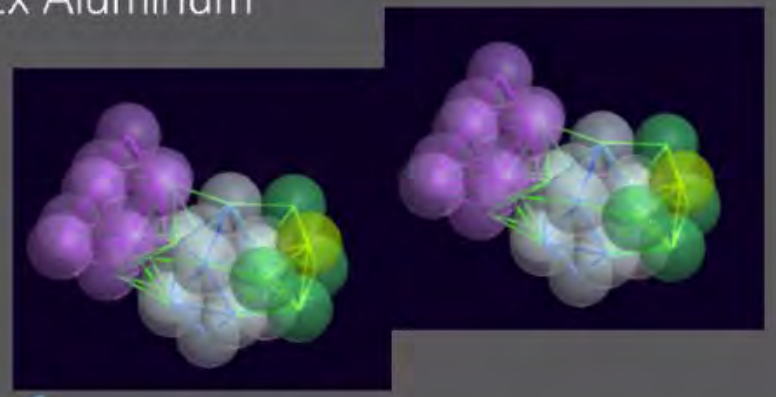


Possible Aureon Reaction

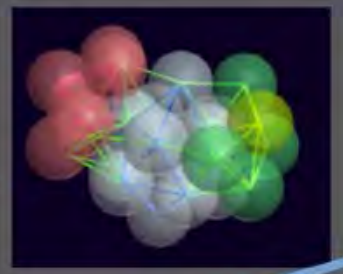
Carbon



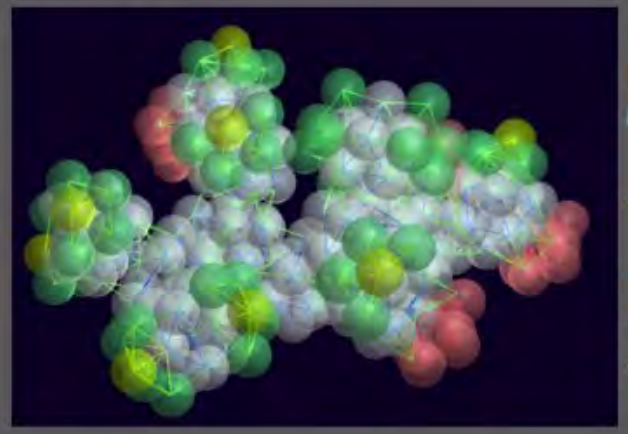
2x Aluminum



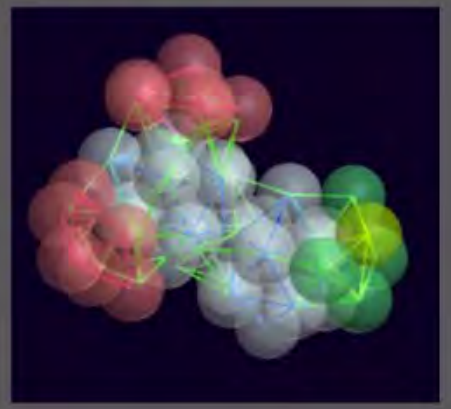
Sodium



Th232

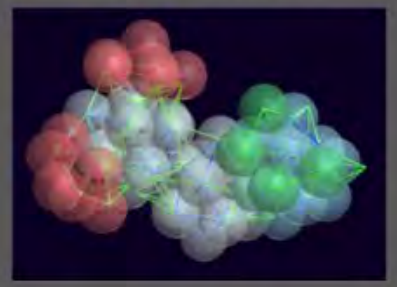


Calcium

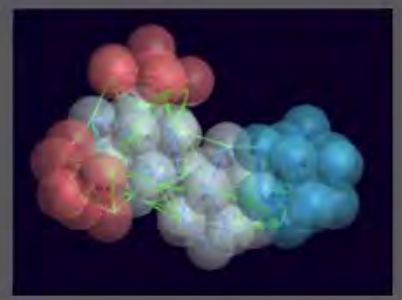


An example break up of Th-232 to daughter elements we see

Chromium



Titanium



Aureon Energy per Reaction

Possible Pathway	Energy per Reaction
Th232 -> C + Ni + Ba + 23n	2 MeV
Th232 -> 2Na + 2Mg + P + Ti + Ni +0n *21 neutrons converted to proton + electron*	216 MeV

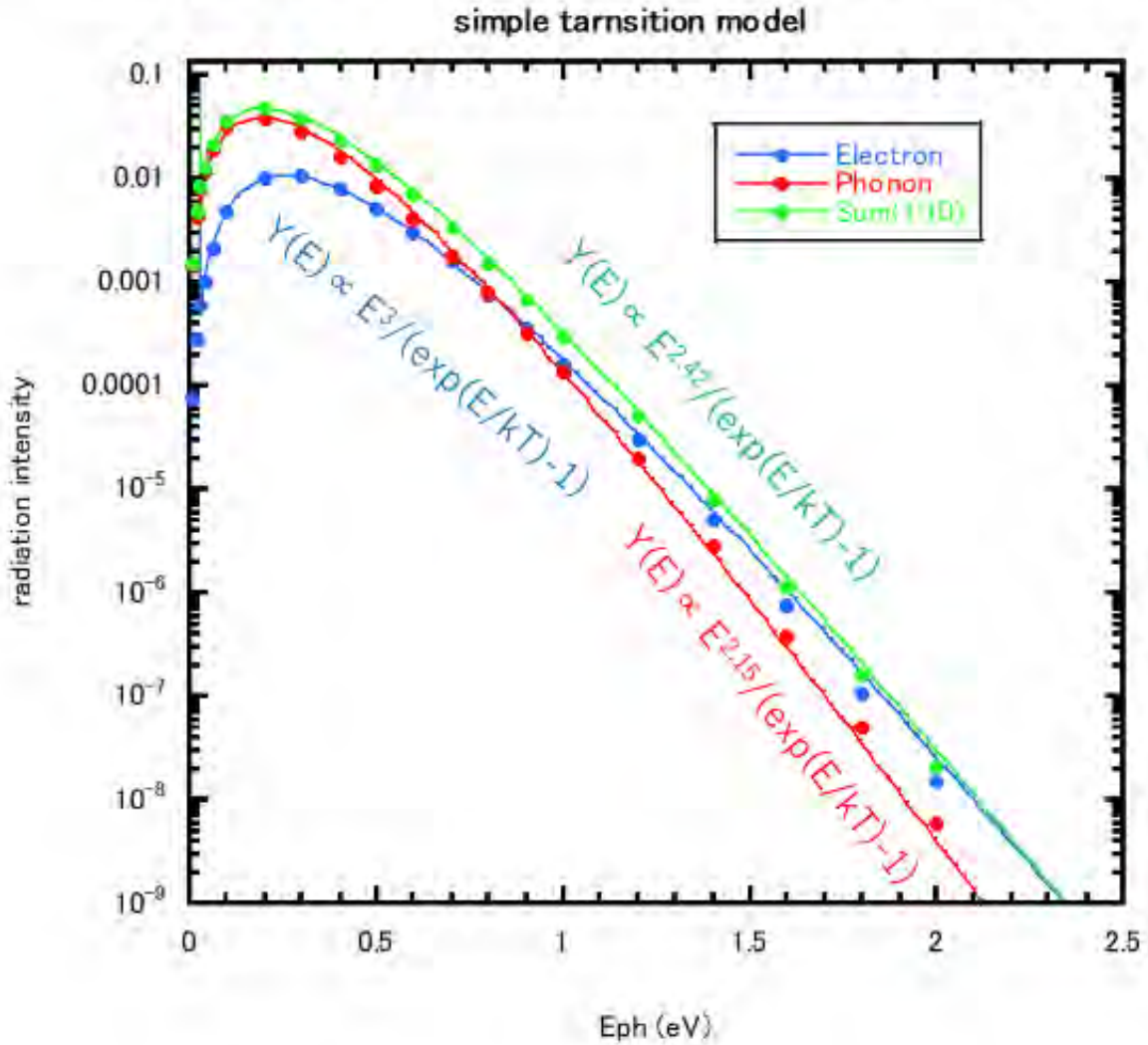
If we have a neutron burst, then low COP
If we have n->p+e conversion, then high COP and electron production

Compare Parkhomov, 1-10MeV per reaction, with 10^{14} reactions per second

Summary

- This suite of experiments was for transmutation research using electro-magnetic stimulation. (Success!)
- Not focused on calorimetry or reaction pathways
- Once we verified energy production and high reaction rate, we stopped, for safety reasons
  - Neutron burst?
  - Let's not melt the lab
  - Aureon team is not expendable

Expected thermal spectrum



Calculated results can be fitted by

$Y(E_{ph}) \propto E_{ph}^{\alpha}/(\exp(E_{ph}/kT)-1)$; parameter α

Electron transitions:

$Y(E_{ph}) \propto E_{ph}^{3}/(\exp(E_{ph}/kT)-1)$

Proportional to black-body radiation, gray-body.

Lattice vibrations (phonon) :

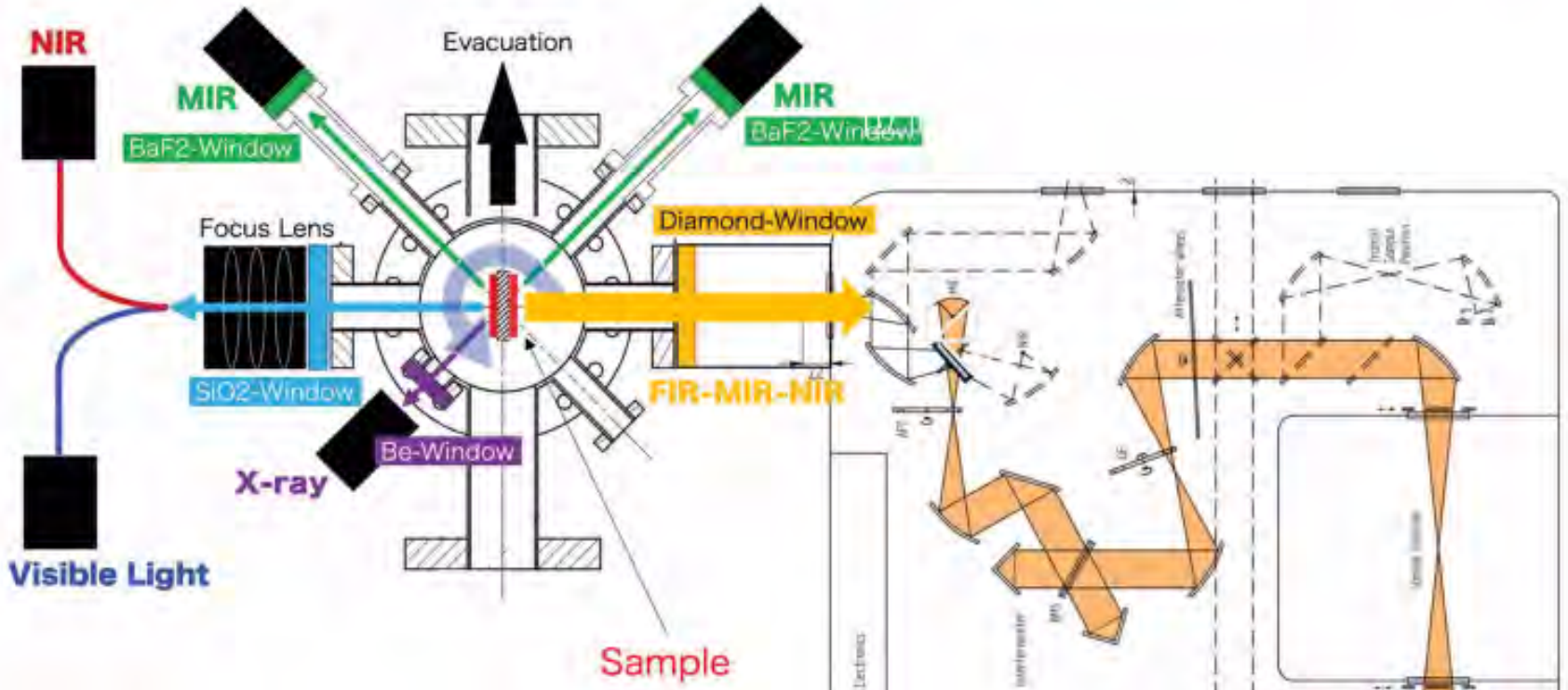
$Y(E_{ph}) \propto E_{ph}^{2.15}/(\exp(E_{ph}/kT)-1)$

The distribution is narrower than that of electrons.

Radiation from metal is the sum of these two.
Not a simple gray-body radiation!
Qualitatively, the high-energy tail reflects the temperature and is driven mainly by electron motion.

Detection System for EM Radiation from Metal Thin Film
— from THz Photons to X-rays Measured by 'BREMS' —

Broad Range ElectroMagnetic wave detection System (BREMS)

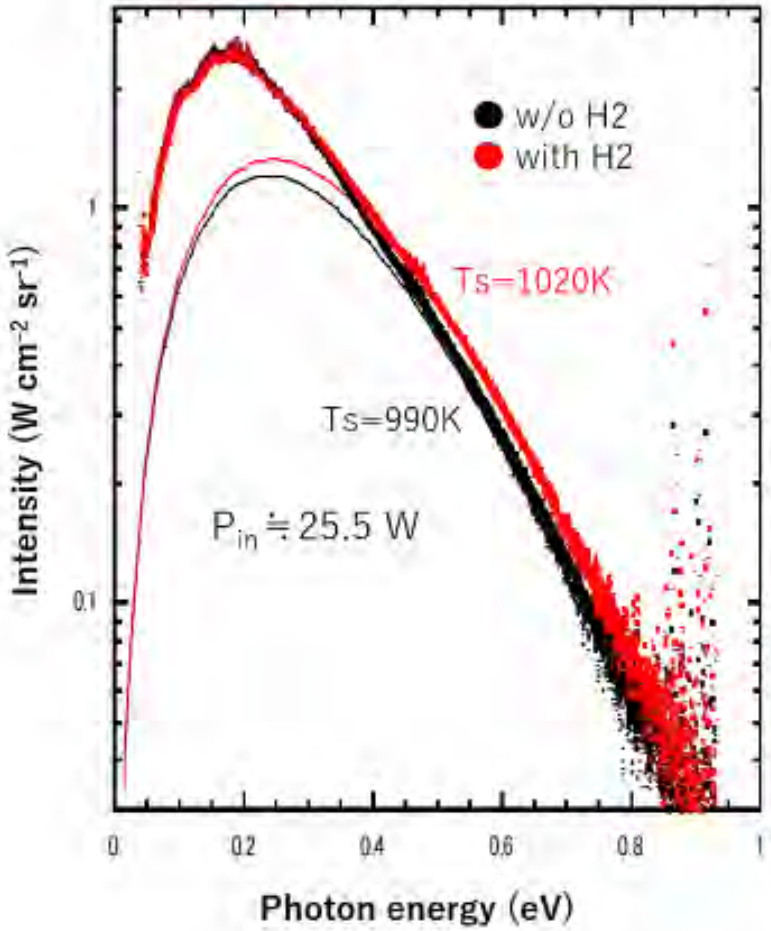


FT-IR device:
INVENIO R (Bruker
MIR mode:
0.043 to 0.93 eV
(28.5 - 1.33 μm)
FIR mode:
0.004 eV to 0.084 eV
(325 - 14.8 μm)

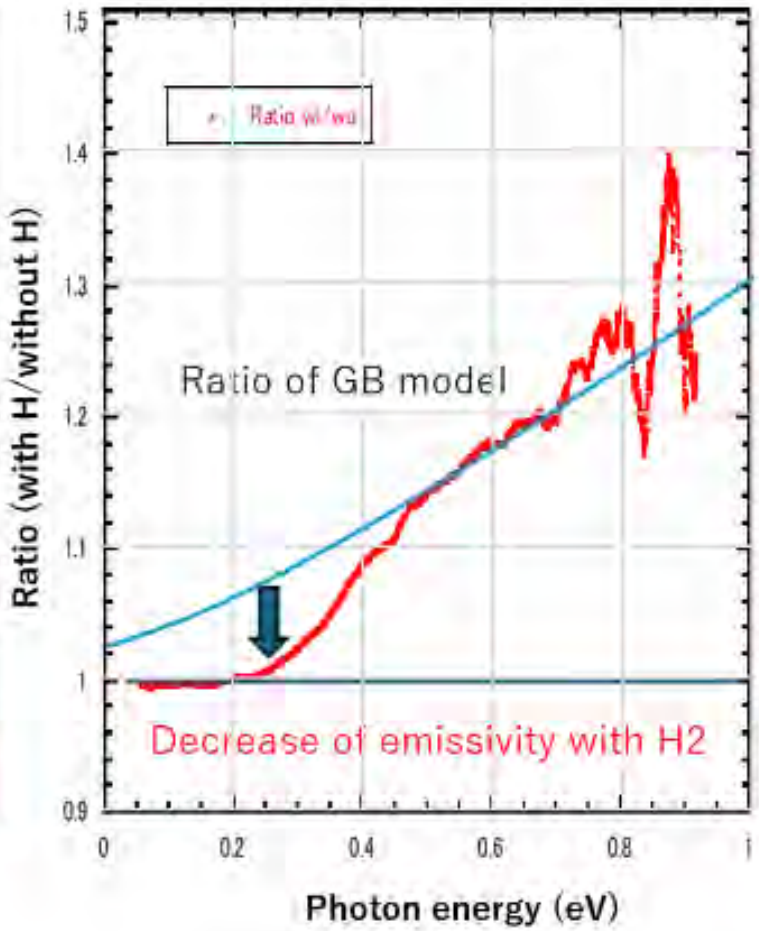
① **MIR:** Mid-infrared region (0.22 – 0.41 eV)
② **NIR:** Near Infrared region (0.5 – 1.13 eV)
③ **Visible Light:** Optical to UV region (1.3 – 5 eV)
④ **X-ray:** hard X-ray region (1 keV – 100 keV)

Sample 058: Comparison between with and w/o H2 gas

Radiation Spectrum



Ratio: with/without H2

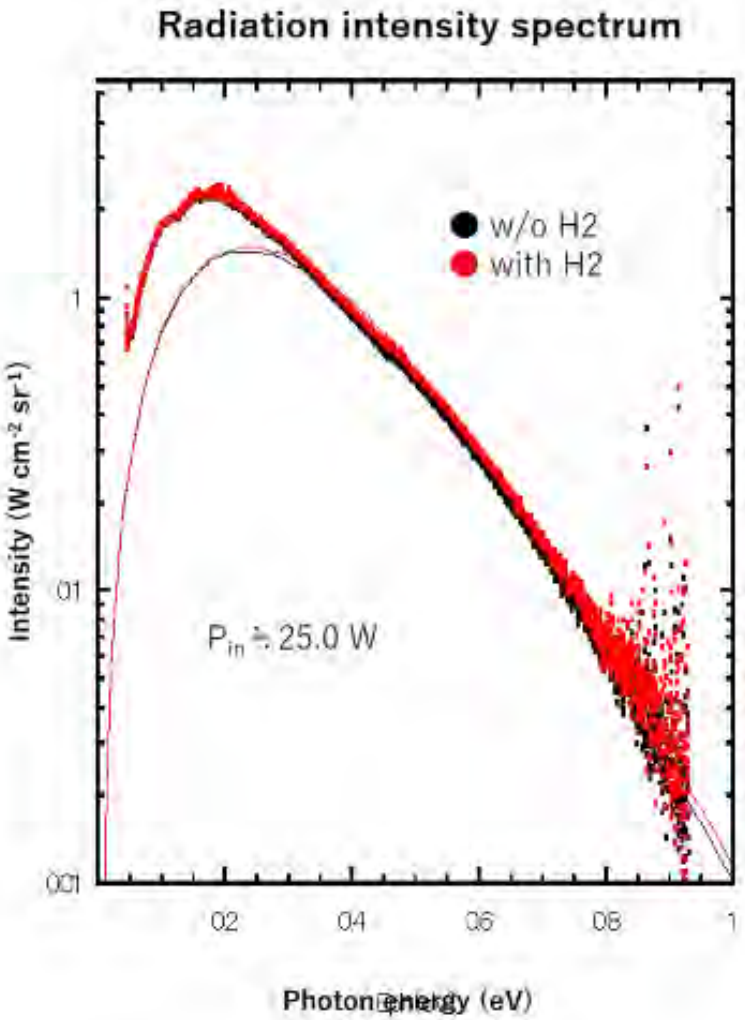


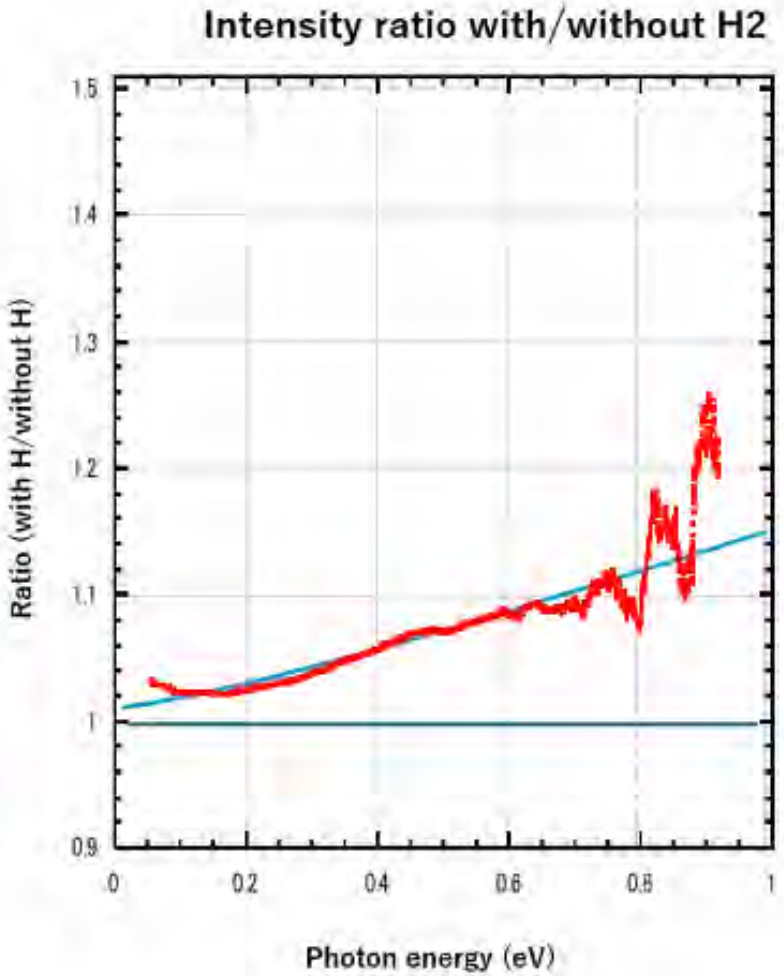
Gray-body model cannot reproduce entire spectrum.
T_s are deduced with data for E_{ph} > ~0.4 eV.

Total radiation increases by about 4% and $\Delta T \sim$ 30K
Increase of the ratio for E_{ph}>0.5 eV corresponds to Gray-body model.

Strong decrease of emissivity for E_{ph} < 0.4 eV is suggested.

Sample 057: Comparison between with and w/o H2 gas





After hydrogen absorption: Although Ts increases only ~10 K, integrated radiation power increases by more than 3%!

The energy dependence of the intensity ratio is in good agreement with the GB model behavior.

Summary

- Without detailed information on the radiation intensity spectrum, it is difficult to reliably quantify unknown thermal power generation.
- Radiation measurements are indispensable for the quantitative evaluation of excess power.
- Compared to the intensity spectrum without H2, the spectrum with H2 exhibits various patterns of enhancement.
- Evaluating excess power only by temperature measurement yields different results from evaluations based on radiation spectra, whether there is a large temperature difference or almost no temperature difference.
- Now, it has become clear that excess thermal power is being generated. The radiation spectrum will provide useful information to study the underlying mechanism.

Physical basis and possible methods for LENR realization and associated hydrogen gas production in ordinary water

Vladimir Vysotskii, Mykhaylo Vysotskyy
Taras Shevchenko National University of Kyiv, Ukraine

To justify such reactions, it is necessary to consider the **main basic requirements for LENR implementation**:

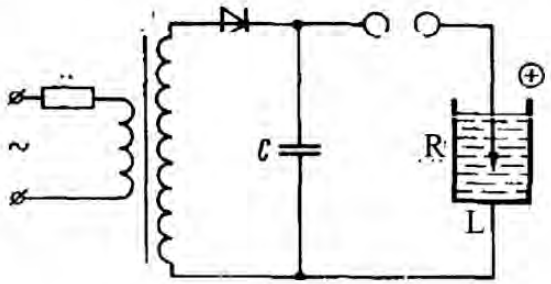
* these reactions must be **exothermic**;
* the daughter products of these reactions must be **stable isotopes**;
* the most efficient reactions should **not contain daughter neutron channels**.

A simple analysis shows that pure natural water exhibits three fusion reactions that satisfy these requirements:

$$O^{18}(0.2\%) + p = \begin{cases} F^{19} + 7.99\,MeV \\ He^{4} + N^{15} + 3.98\,MeV \end{cases};$$

$$O^{16}(99.76\%) + O^{16}(99.76\%) = S^{32} + 16.54\,MeV$$

One of the typical schemes for implementing electrohydraulic effect is shown in Fig. [L..A. Yutkin. Electrohydraulic Effect and Its Application in Industry, 1986]



The electrohydraulic effect is characterized by the energy release in the active resistance R of the discharge circuit in the volume of water, the value of which is close to the critical condition

$$R^2 \approx 4L/C$$

Here C is the capacitance of the capacitor in the electric discharge circuit, R and L are the active resistance and inductance of the discharge circuit.

The typical parameters of the electrohydraulic effect

The typical total duration of such a discharge current pulse is a few microseconds or fractions of a microsecond, with a leading edge of 1-3 nanoseconds.

The instantaneous power at the leading edge of the current pulse can reach 300-5000 kW.

The steepness of the leading edge of the current pulse determines the rate of expansion of the discharge channel. When a voltage of 10-50 kV is applied to the discharge electrodes, the current pulse amplitude reaches 10-50 kA.

At the **initial stage of the pulse, atoms are ionized, forming a plasma cord**. The subsequent portion of the discharge current rapidly heats this cord to a temperature of 15,000-20,000 K, leading to the ionization and evaporation of water molecules and their atoms and a very sharp increase in pressure.

Nuclear fusion stimulated by an accompanying magnetic field in a gas cavity near the discharge zone

The rapid growth and high pressure in the gas cavity around each discharge streamer with a strong internal electric current are accompanied by the synchronous dissociation of water molecules and the ionization of these molecules and atoms. It is well known that the motion of a charged particle in a magnetic field is equivalent to a 2D harmonic oscillator, and in a variable field, to a non-stationary harmonic oscillator with a frequency

$$\omega(t) = |q|H(t)/Mc$$

and an instantaneous equidistant spectrum of eigenfunctions

$$E_n = \hbar\omega(t)(n+1/2),$$

$$\Psi(x, r_s, t \geq 0) = \sum_n B_n(r_s)\Psi_n(x)e^{-iE_n t/\hbar}e^{-\varphi_m},\ \Psi_n(x) = C_n H_n(x)e^{-x^2/2x_0^2}$$

When a pulsed electric discharge current with a **very short leading edge** and a longer trailing edge flows, a similar magnetic field is formed and the frequency of this oscillator changes

$$\omega = \omega_0(1+f(t)),\ \ f(t) = 0,\ t < t_0,\ \ f(t) \approx ge^{-(t-t_0)/\tau},\ t \geq t_0$$

This pulse discharge mode leads to short-term **synchronization of the eigenfunctions** and the **formation of a coherent correlated state** of this particle, which leads to very large and comparatively long fluctuations in the momentum and energy of the particle, the amplitude of which corresponds to the Schrödinger-Robertson uncertainty relations

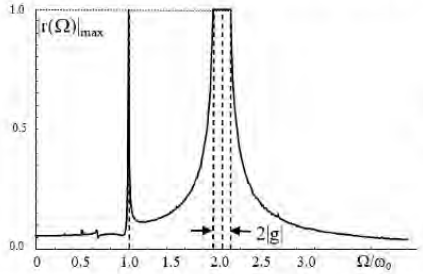
$$\delta q \delta p \geq \hbar/2\sqrt{1-r^2} \equiv \hbar^*/2,\ \hbar^* = G\hbar, G = 1/\sqrt{1-r^2},\ \delta A = \sqrt{\sigma_A},$$

$$\delta E \delta t \geq \hbar/2\sqrt{1-r^2} \equiv \hbar^*/2,\ \hbar^* = G\hbar,\ G = 1/\sqrt{1-r^2},$$

$$\delta E^{(\min)} = (\delta p)^2/2M = G^2\hbar^2/8M(\delta q)^2 \equiv (\hbar^*)^2/8M(\delta q)^2$$

Here r is the correlation coefficient ($0 \leq |r| < 1$), G is the coefficient of correlation efficiency ($1 \leq G < \infty$).

This condition corresponds to the realization of **parametric resonance**, excitation of the CCS, in which **the frequency Ω of the most intense (control) spectral Fourier component $H(\Omega)$ of the non-stationary magnetic field of the discharge current is 2 times greater than the frequency ω of ion oscillations in the magnetic field.** The conditions and efficiency of parametric and direct resonances in the formation of a CCS are shown in the figure.



$$\omega = \omega_0(1 + g\cos\Omega t)$$

If the amplitude of the magnetic field within the gas cavity is significantly greater or less than the optimal value, then the process of formation of the CCS will be weakened, which leads to significantly smaller energy fluctuations and a low probability of nuclear fusion involving protons and oxygen nuclei.

Water molecules have two basic vibrational modes, which can form coherent correlated states:

a) **symmetric stretching vibrations** with a frequency of $1.1\cdot10^{14}$ Hz, in which the O–H bonds simultaneously lengthen and shorten.

b) **antisymmetric stretching vibrations** with a frequency of $1.14\cdot10^{14}$ Hz , in which one O–H bond lengthens and the other synchronously shortens.

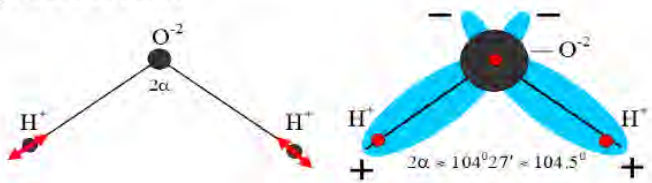


Fig. Normal stretching vibrations of a proton in a water molecule

The main nuclear reactions $O^{18} + p = F^{19}; He^4 + N^{15}$ are activated by protons located in natural potential nanowells 5.1 eV deep, located 0.96 Å from the oxygen nucleus within the water molecule, using these symmetric and antisymmetric proton stretching oscillations.

An additional result of these reactions is **the "liberation" of one proton from a water molecule**, which can be converted into a free hydrogen atom.

This system corresponds to the following parameters:

$$u \approx 4.5 \cdot 10^3 \,\mathrm{m/s},\ \Delta t_{\min} \approx (1-3) \cdot 10^{-14} \,\mathrm{s},\ \omega \Delta t_{\min} \approx (1-3)$$

The main parameter is several times larger than the optimal value $\omega_{\max} \tau \approx 0.6-0.7$, which corresponds to a lower correlation efficiency coefficient and a lower probability of nuclear fusion. On the other hand, this probability remains large enough for practical application.

Conclusion

These studies have shown that water, when exposed to electrical discharges, can be a fairly effective medium for controlled nuclear fusion at low energies.

These reactions can be stimulated both by the **action of the pulsed magnetic field of the discharge on the nascent** ions and by the **direct action of acoustic shock waves on the water molecules**. The efficiency of these reactions can be significantly increased by **using salt water or water with other dissolved components**. The main challenge is to create optimal high-voltage discharge conditions with the **shortest possible leading edge**.

A **byproduct of these reactions is the formation of free hydrogen**, which is formed (freed from oxygen bonds) during water fusion.

The previously discussed method of implementing LENR in a water volume with conventional cavitation of a high-pressure water jet [A.I.Koldamasov, A.A.Kornilova, V.I.Vysotskii et al. *Observation and investigation of nuclear fusion and self-induced electric discharges in turbulent liquids.* ICCF12 Proceedings, (2006), pp.97-107.] is much less effective due to significantly lower cavitation energy.

Electrodynamic mechanism of direct energy transfer from fast daughter LENR fusion isotopes to electric current in the E-Cat system

Vladimir Vysotskii, Mykhaylo Vysotskyy
Taras Shevchenko National University of Kyiv, Ukraine

The formation of excited atom leads to the creation of its **paramagnetic moment**:

$$M_a \approx \mu_B \sqrt{l(l+1)}$$

Here μ_B=10^{-23} J/T is Bohr magneton, l is an orbital electron quantum number.

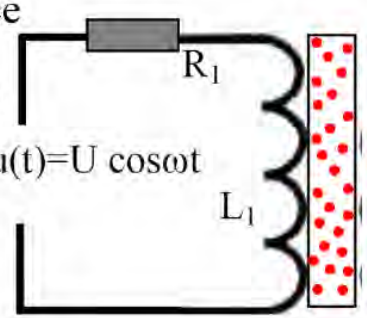
A non-stationary ensemble of excited atoms in a gaseous medium at temperature T corresponds to the formation of a non-stationary thermodynamic-equilibrium paramagnetic susceptibility (Curie-Weiss law)

$$\chi(t) = \mu_o n_a^*(t) < (M_a^{(n)}(t))^2 >_n /3kT$$

and magnetic permeability within an external inductance

$$\mu(t) = 1 + \chi(t)$$

Here, $\mu_0 = 4\pi\square 10^{-7}\ H/m$ is the magnetic constant, $n_a^*(t)$ is the time-dependent concentration of excited atoms.



A change in magnetic permeability leads to a change in the inductance of the coil (solenoid):

$$L_1(t) = L_{10}\{1 + \chi(t)\}$$

In an quasi-stationary stochastic uncorrelated nuclear fusion regime with $<n_a^*>$ = *const*, the solenoid's inductance has constant value:

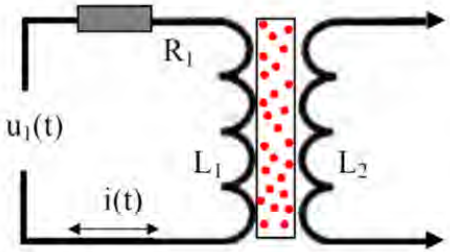
$$L_1 = L_{10}\{1 + < \chi >\}$$

In such a quasi-stationary system, the current energy and power of the solenoid's magnetic field for an alternating current $i(t)=J(t)\cos(\omega t)$ are determined by the standard expressions:

$$W_M = L\{i(t)\}^2 / 2$$

$$P_M = dW_M / dt = Li(di / dt)$$

In the presence of a secondary coil with inductance L_2 surrounding the same nuclear-active chamber, the changes in this magnetic energy, power and field lead to the release of energy and power in the secondary coil with corresponding ohmic losses P_{loss}. This corresponds to a **standard transformer with two magnetically coupled coils.**



In such a standard (quasi-stationary) transformer, **no additional energy is released**, but rather a simple transfer of energy from the primary coil to the secondary takes place with associated ohmic losses.

2. Conversion of kinetic energy of nuclear daughter isotopes into electrical energy in active transformers

The situation changes radically in the case of non-stationary global modulation of the inductance. In this case, the inductance $L_I(t)$ is a non-stationary function and the total magnetic field power

$$P_M = Li(di / dt) + i^2 (dL / dt) / 2 = P_{MJ} + P_{ML}$$

inside the solenoid includes an additional component

$$P_{ML} = \{i(t)\}^2 L_{10} (d\chi(t) / dt) / 2$$

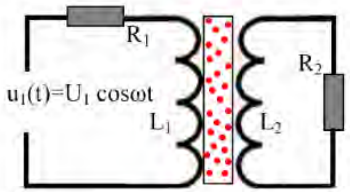
that depends on the controlled change in magnetic susceptibility, formed under the influence of the alternating magnetic field on the nuclear fusion. In such an active transformer, the power transferred to the secondary coil, has **three components** corresponding to absorption or gain: a) input current $i(t)$; b) fusion-related oscillating susceptibility $\chi(t)$; c) ohmic losses in both coils and in a load with resistances R_1 and R_2:

$$P_{\text{sec}} = P_{MJ} + P_{ML} - P_{loss}$$

This inductive component P_{ML} can be an efficient source of electrical energy in the system under consideration.

Kirchhoff's equations for both closed loops have the following form: $u_1 = R_1 i_1 + \frac{d}{dt}(L_1 i_1 + M_0 i_2)$,

$$0 = R_2 i_2 + \frac{d}{dt}(L_2 i_2 + M_0 i_1)$$



From these equations, we get the time-averaged complex impedance $Z_{eff} = R_1 + \frac{\omega^2 M_0^2}{R_2} - \frac{g\omega}{2} L_{10} \sin\varphi$ of the primary coil under the resonant modulation condition Ω=ω for the magnetic susceptibility.

In this formula, the additional component $-\frac{g\omega}{2} L_{10} \sin\varphi$, under the condition $\sin(\varphi) > 0$, corresponds to the effective **negative resistance** associated with the influence of the changing magnetic permeability of the working medium in the resonant system.

The input power of such a transformer is equal to $P_1 = \frac{U_1^2}{2Z_{eff}} = \frac{i_1^2 Z_{eff}}{2}$

The current in the secondary coil and the output power of this transformer are described by the formulas

$$i_2 = \frac{\omega M_0}{R_2} i_1, \quad P_2 = \frac{1}{2} R_2 i_2^2 = \frac{1}{2} \frac{\omega^2 M_0^2}{R_2} i_1^2$$

From these formulas we obtain the final ratio (**effectively the COP**) of the output to input power of the active transformer

$$\frac{P_2}{P_1} = \frac{\frac{\omega^2 M_0^2}{R_2}}{\frac{\omega^2 M_0^2}{R_2} - \{\frac{g\omega}{2} L_{10} \sin\varphi - R_1\}}$$

when the resonant modulation condition is met, i.e. when the frequency of the initial current in the primary coil and the frequency of the change in susceptibility coincide.

This formula shows that the process of efficient conversion of nuclear fusion energy into electrical energy and the generation of additional electrical energy through resonant modulation of magnetic susceptibility occures when threshold conditions are met:

$$g\omega L_{10} \sin\varphi > 2R_1, \sin\varphi > 0$$

From this expression it is clear that the ratio of output to input powers during optimal resonant pumping does not depend on time.

Conclusion

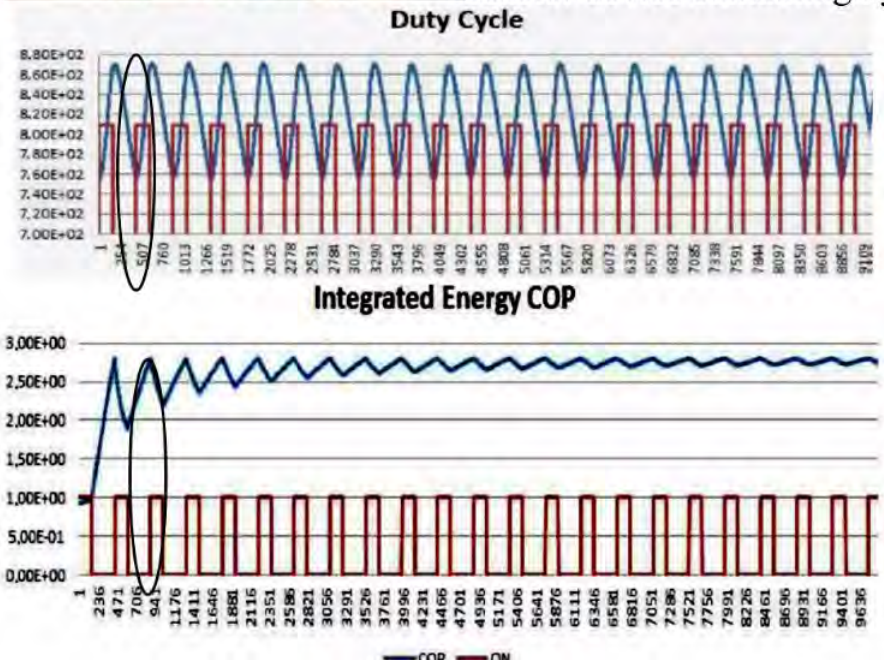
From these conditions, it becomes clear that the implementation of such an active transformer mode with the **conversion of LENR nuclear energy into electrical energy** can be achieved in a system of two coaxial coils surrounding a nuclear-active medium under the following conditions:

- **synchronization of periodic LENRs in time in the all volume of the working chamber;** ;\
- **high turn density** N_{coil}/l_{coil} of the first coil**;**
- **low active resistance** of this coil;
- **relatively low temperature of the nuclear-active medium**, which is automatically realized in E-cat systems, where the energy of nuclear fusion is not converted into heat, but directly into electric current;
- **high final power output** of the active medium used.

A similar effect (phase lag of the released energy relative to the input energy) was observed in previously conducted independent successful experiments



Replication of E-Cat HT Dec. 2012 - March 2013 Giuseppe Levi, Evelyn Foschi, Torbjörn Hartman, Bo Höistad, Roland Pettersson, Lars Tegnér, Hanno Essén. Indication of anomalous heat energy production in a reactor device containing hydrogen-loaded nickel powder

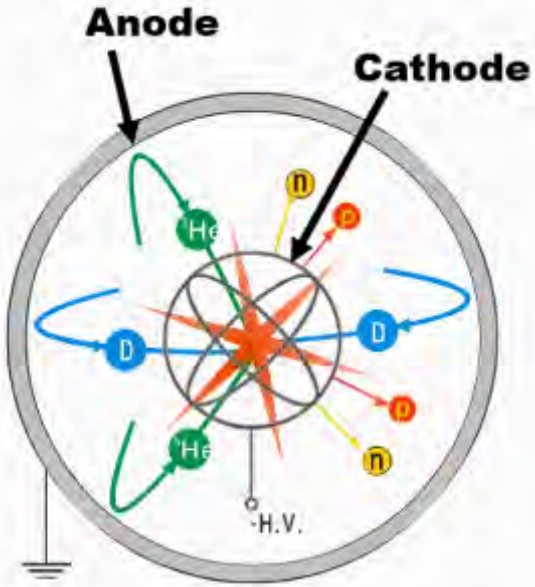


Periodic switching of the heating coil on and off **by pulses of direct current.**

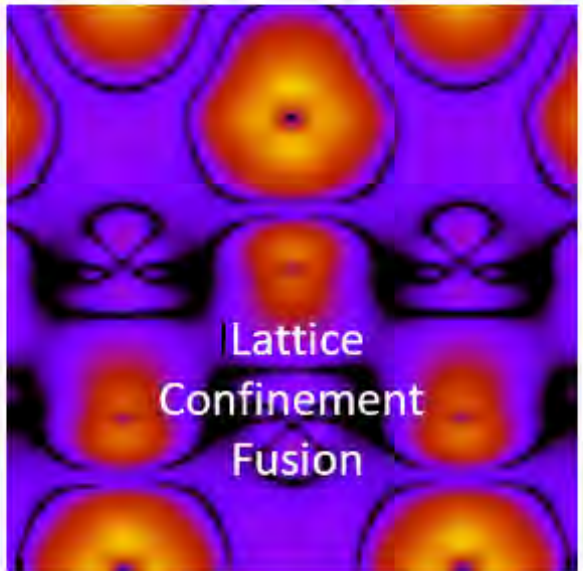
Phase delay (time delay) of the nuclear reaction and energy release relative to the stimulating electric current and magnetic field.

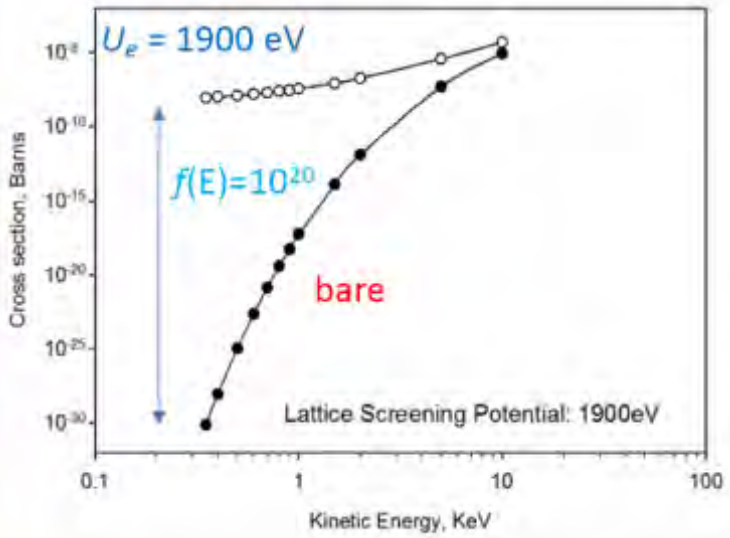
Outline

- Overview of Astral Systems
- Multi-State Fusion
  - Inertial Electrostatic Confinement Fusion
  - Lattice Confinement Fusion
- Enhanced Neutron Yields
  - Cathode Design Study
  - LCF Materials Study
- Summary



IEC





Overview of Astral Systems

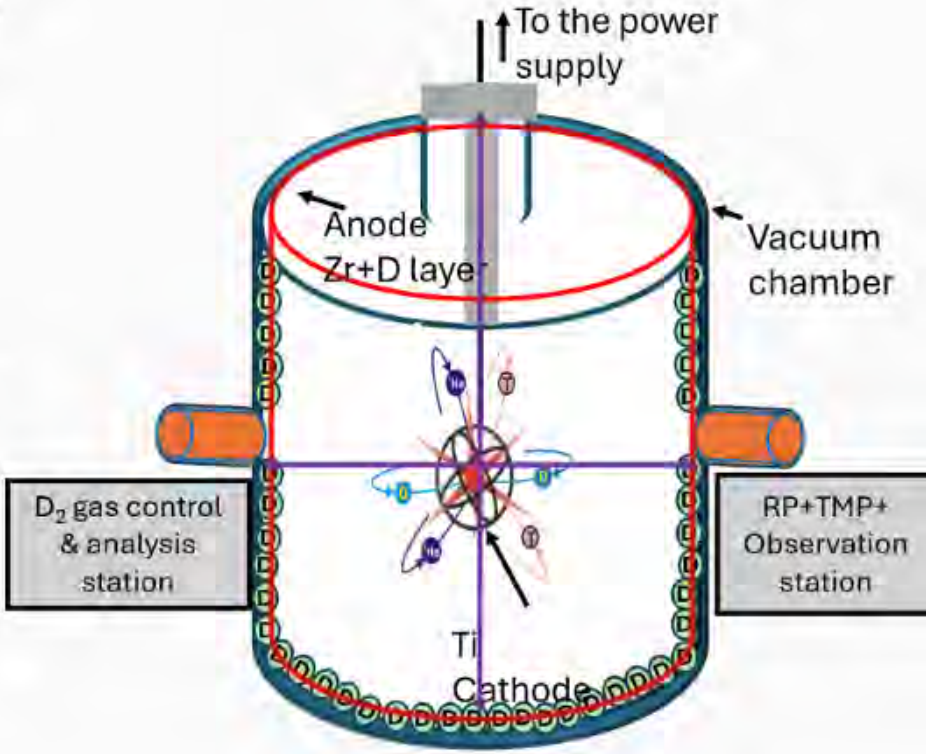
- Transformative fusion technology
- Neutron Irradiation
  - Largest volume, continuously operable high-energy fusion volumetric neutron source
  - Access to both D–D (2.45 MeV) and D–T (14.1 MeV) neutron sources
- Applications
  - Material Qualification and Regulatory Validation
  - Neutron Damage & Durability Testing
  - Radiation Hardness Testing
  - Neutron Activation Analysis
  - Neutron Radiography
- www.astralsystems.com



От Jed Rothwell всем
Can't hear!

Multi-State Fusion (MSF)

- Inertial Electrostatic Confinement (IEC) Fusion[1]
  - Concentric cathode connected to a negative bias and is surrounded by a grounded anode
- Lattice Confinement Fusion (LCF)[2]
  - Deuterated metals are used as an electrode in the IEC system to enact LCF fusion reactions
- Two fusion technologies work in tandem to create an increased number of fusion events compared to each technology alone
  - MSF enhances neutron production rate (NPR) and transfers concentration of the fusion events from the cathode to the inner surface/anode of chamber.



1. Robert Hirsch, "Inertial-Electrostatic Confinement of Ionized Fusion Gases", Journal of Applied Physics, Volume 38(11), Pages 4522-4534 (1967), https://doi.org/10.1063/1.1709162
2. Theresa L. Benyo, L. Forsley, and B. Steinetz, "The History of LENR Research at NASA Glenn Research Center", Journal of Condensed Matter Nuclear Science 38 (1): 13–41 (2023),

Inertial Electrostatic Confinement Fusion

- High voltage electric fields used to accelerate and confine ions into a dense core creating plasma
- Cathode and anode configuration shown in Fig 1a to the right
- Simple design fusor consists of two concentric metal spherical grids.
- Kyoto Univ team research led by Mahmoud Bakr[3]
  - Fig 1: IEC-17 diagram
  - Fig 2: IEC-17 -> increased neutron yields aka neutron production rates (NPR) with higher cathode voltages
  - NPR increases linearly with applied current

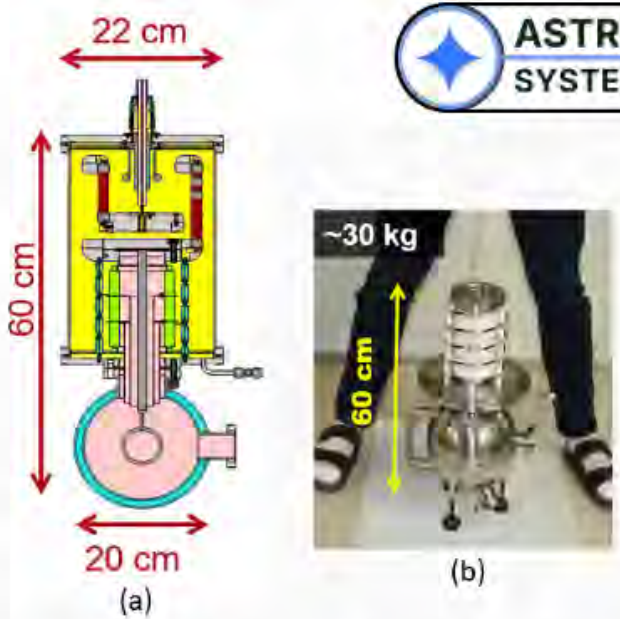


Figure 1. IEC Diagram: (a) IEC-17 portable system for nuclear security applications; (b) photo of the IEC-17.

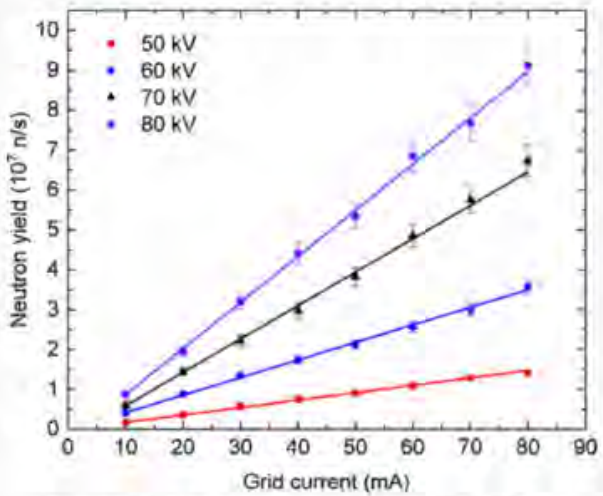
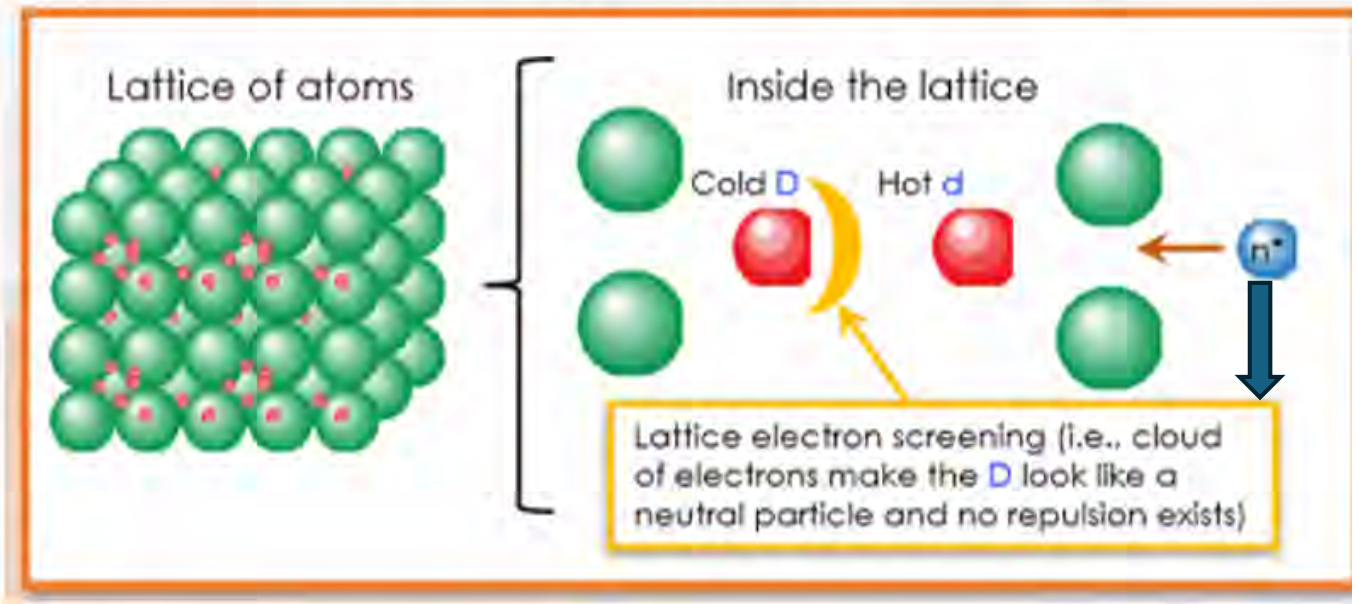


Figure 2. Neutron yields from IEC-17 as a function of grid current at 50, 60, 70, and 80 kV cathode voltages

3. Mahmoud Bakr, et al, "Characterization of an ultra-compact neutron source based on an IEC fusion device and its prospective applications in radiography", Fusion Engineering and Design, Volume 167, 112346 (2021), https://doi.org/10.1016/j.fusengdes.2021.112346

Lattice Confinement Fusion

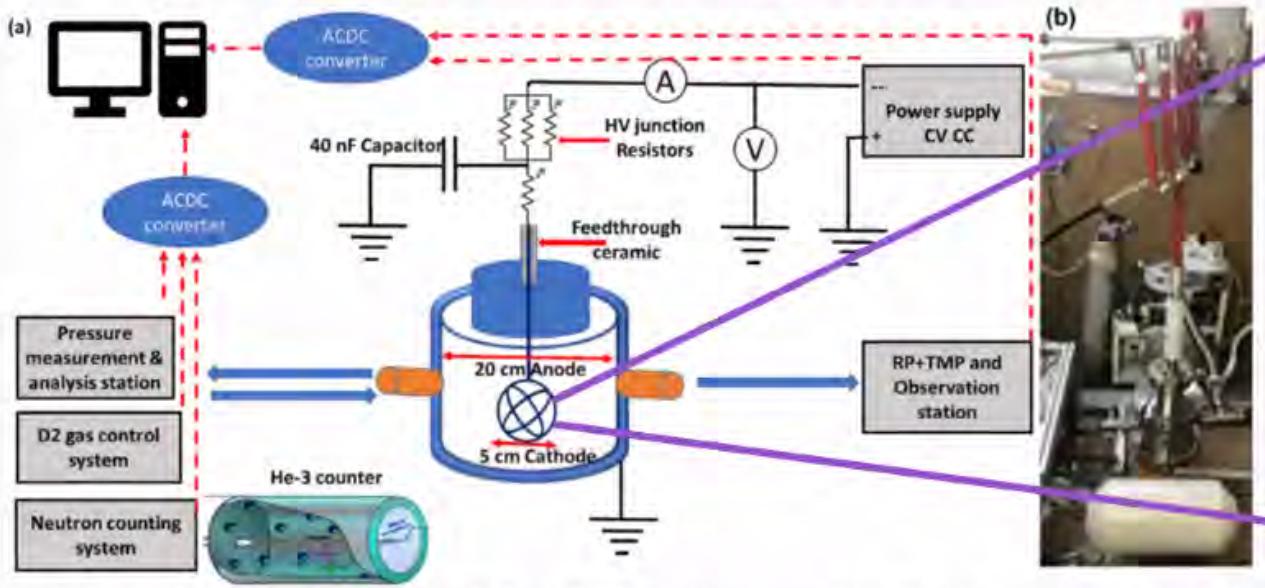
- Deuterated metals hold the fusion fuel
- Electrons from metals provide electron screening
- Various triggers; electric current, plasma, x-ray, gamma ray enable LCF
  - For gamma ray irradiation deuterated metals; gamma beam photo-dissociates some of the deuterons in the metal lattice creating proton-neutron pairs
  - Allows energized photo-dissociated neutrons to transfer K.E. to resting deuterons in lattice which then fuses with another resting deuteron with the help of electron screening.
- NASA team lead by Bruce Steinetz conducted gamma irradiation experiments to show evidence of electron-screened DD fusion[4]



4. Bruce Steinetz, et al, "Novel Nuclear Reactions Observed in Bremsstrahlung-Irradiated Deuterated Metals", Phys. Rev. C, Volume 101, 044610 (2020), https://doi.org/10.1103/PhysRevC.101.044610

Enhanced Neutron Yields: Cathode Design Study[5]

- Eleven cathodes were fabricated from stainless steel in three different groups with different transparency and number of apertures.
- NPRs were investigated as a function of the cathode transparency and number of apertures at low power operating mode ~1 kW.



The experimental layout of the IECF system used in the investigations (a) and a photograph of the experimental setup (b).



View of cathode with circular openings while in operation.

5. Mahmoud Bakr, et al, "Influence of electrodes' geometrical properties on the neutron production rate of a discharge fusion neutron source", Phys. Plasmas 30, 032701 (2023); https://doi.org/10.1063/5.0134631

Enhanced Neutron Yields: LCF Materials Study

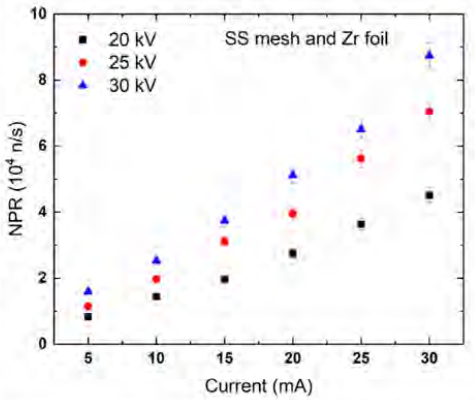
- LCF Materials Study Conclusions[6]
  - Higher neutron production rates are achievable using Zr mesh anodes compared to SS mesh anodes.
  - Performance enhancement is attributed to surface fusion or lattice confinement fusion occurring between neutrals and D atoms deposited on the mesh surface in Zr is higher than in SS.
  - Pre-loaded D on the ZrD mesh material further increased the neutron production rate compared to the Zr mesh, due to the concentration of D on the mesh surface increasing the probability of fusion events with neutrals generated from charge exchange in the MSF system.

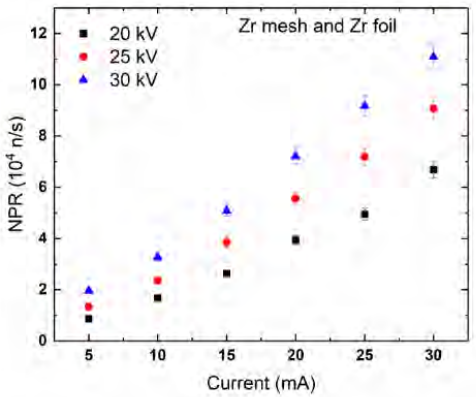
6. Mahmoud Bakr, et al, "The Effect of Electrode Materials on the Fusion Rate in Multi-State Fusion Reactors", Materials Volume 18, 3734 (2025), https

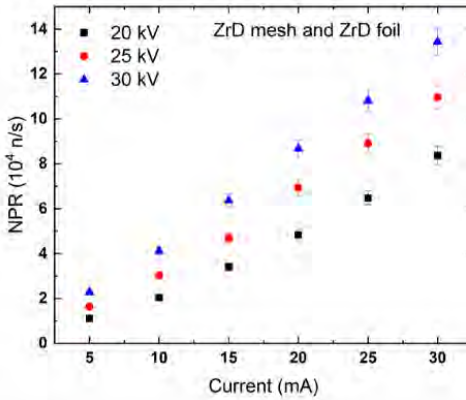
Astral Systems |

Enhanced Neutron Yields: LCF Materials Study

- Results[6] -> increase in NPR due to LCF
  - Zr mesh anodes produced higher NPRs than SS mesh ones, reaching 1.294 times at 0.9 kW.
  - These processes were further modified by the deuterium pre-loading in the ZrD anode and produced 1.588 times n/s at 0.9 kW compared to 'SS mesh and Zr foil'







6. Mahmoud Bakr, et al, "The Effect of Electrode Materials on the Fusion Rate in Multi-State Fusion Reactors", Materials Volume 18, 3734 (2025), https://doi.org/10.3390/ma1816373

Background : Principle of focusing compression due to super-multi-jets colliding proposed by our laboratory

- ✓ The point compression principle, based on focusing due to collision of super-multi-jets in pulses, generates extremely high-temperature and high-pressure regions around the collision point, because increase of the number of jets colliding leads to higher compression (Fig 3).

K. Naitoh, patents. 2010-2026.

- ✓ The-high-temperature and high-pressure H_2 generated by this principle was supplied onto metal powder, primarily based on Pd, Cu, and Ni.

- ✓ We have hypothesized this principle could promote exothermic reactions.

K. Naitoh et al., *J. Condensed Matter Nucl. Sci*. 24, 2017

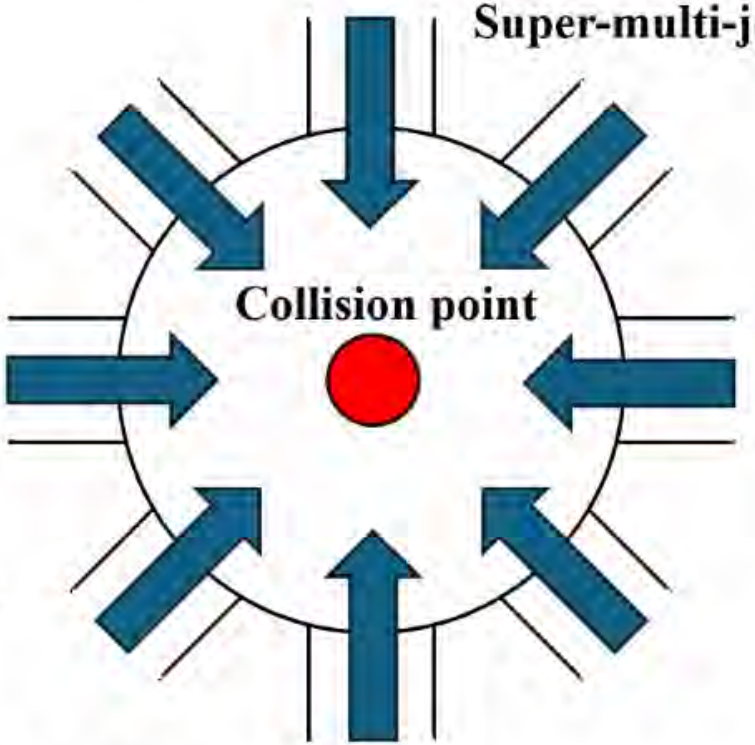


Fig 3. Principle of focusing compression due to super-multi-jets-colliding

Background : Our previous research

- ✓ We developed a reactor capable of colliding a single H_2 jet onto a sample. Based on the mirror image principle, this reactor can reproduce the collision of two opposing jets (Fig 1).

  T. Kobayashi et al., *J. Condensed Matter Nucl. Sci*. 36, 2022

- ✓ A positive correlation was observed between the H_2 injection pressure ($\leq$ 1.0 MPa) and temperature rise (Fig 2).

- ✓ When the H_2 injection pressure was increased to 8.1 MPa, further heat generation was observed (Fig 2) .

  T. Kobayashi et al., *JCF23*, 2023
  T. Kobayashi et al., *J. Condensed Matter Nucl. Sci*. 38, 2024

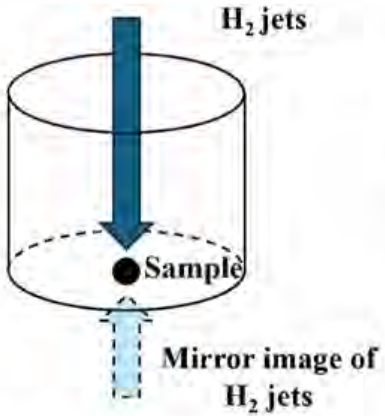


Fig 1. Image of two opposing jets colliding

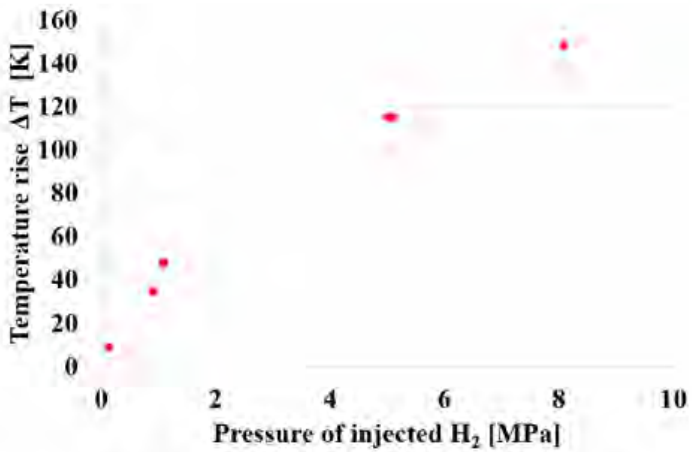


Fig 2. Relationship between the H_2 injection pressure and temperature rise

Conclusion & Outlook

Conclusion

- ✓ We conducted experiments injecting H_2 at up to 14.1 MPa to CNZ powder using the principle of focusing compression due to super-multi-jets colliding.
- ✓ Comparing the H_2 injection pressures of 8.1 MPa and 14.1 MPa, the latter condition resulted in an increased sample temperature rise, as well as greater heat generation and heat output.
- ✓ Estimating the anomalous heat from the sample's temperature rise revealed that the heat output per unit mass for CNZ was greater than that of PNZ.

Outlook

- ✓ We plan to conduct experiments at the higher H_2 injection pressure to confirm more heat generation.
- ✓ We are considering to improve the experimental system to achieve higher-frequency pulsed injection.

Background : New reaction chamber applied with the principle of focusing compression of super-multi-jets colliding

- ✓ A single H_2 jet injected from the top of the chamber hit on the quartz glass and diverges toward the wall of the chamber.
- ✓ The H_2 diverged jets go down along the wall.
- ✓ The H_2 diverged jets converge to the center point as super-multi-jets to collide.
- ✓ The high-temperature and high-pressure H_2 region generated by the collision was supplied the sample right below the collision point.

T. Kado et al, *ICCF26*, 2025

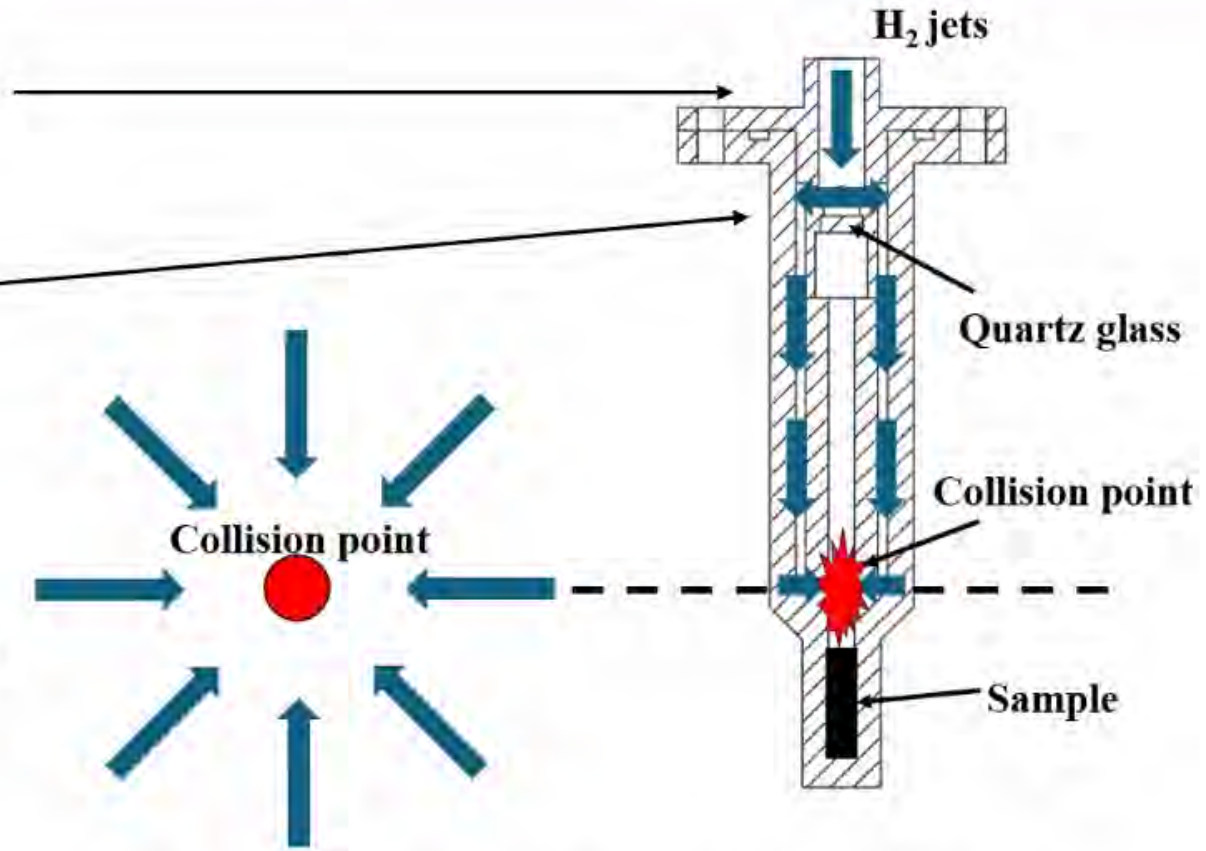


Fig 4. The new reaction chamber

Experiment Overview

Experimental Approach

- H_2 injection pressure : **8.1 MPa or 14.1 MPa**
- Number of pulsed injection times : **1 or over 20**

These experiments were conducted at the Shiraoi Test Site of the Aerospace Systems Center, Muroran Institute of Technology.

Table 1. Experimental conditions

Sample	CNZ（Cu-Ni-Zr alloy）
Sample mass	1.0 g
Set preheated temperature	573 K
gas	H_2

Comparison with heat outputs with PNZ powder and Cu powder (Single pulsed injection of hydrogen super-multi-jets)

- ✓ The heat output per unit mass using CNZ was more than ten times greater than that of previous PNZ.
- ✓ The total heat generation of Cu measured includes the heat generated by the reduction and sintering processes of Cu. These chemical heat generations are eliminated based on two assumptions as follows.
  - ✓ The outer 5 nm of 100 nm Cu particles is oxidized (CuO) [10]. S. Suzuki, and M. Isshiki, *Materia*, 1998
  - ✓ Cu powder sintering occurs due to the high-pressure H_2 injection and exothermic reaction.

Table 4. The anomalous heat generations and outputs with PNZ, Cu, and CNZ

Sample	PNZ	Cu	CNZ	CNZ
Sample mass	3.0 g	1.0 g	1.0 g	1.0 g
Set preheated temperature	573 K	573 K	573 K	573 K
H_2 injection pressure	8.1 MPa	8.1 MPa	8.1 MPa	14.1 MPa
Heat generation Q	**231 J[1]**	**69.1 J[2]**	**49.5 J[2]**	**65.3 J[2]**
Heat output W	**0.0192 kW/g-PNZ**	**1.38 kW/g-Cu**	**1.27 kW/g-CNZ**	**1.45 kW/g-CNZ**

[1] T. Kobayashi et al., *JCF23*, 2023
[2] Y. Suzuki et al., *JCF-Proceedings*, 2026

Continual Pulsed Injection Experiment using CNZ (Continual pulsed injection of hydrogen super-multi-jets over 40 times)

✓ Pulsed H_2 was injected into CNZ at 1.1 sec intervals continually for over 40 times.

- The first 5 pulsed injections recorded a temperature rise over 100 K.
- 20 out of 40 pulsed injection showed a temperature rise over 50 K.

Table 5. Experimental conditions

Sample	CNZ
Sample mass	1.0 g
Set preheated temperature	573 K
gas	H_2
Injection Pressure	12.1 MPa
Frequency	40 times
Interval	1.1 sec

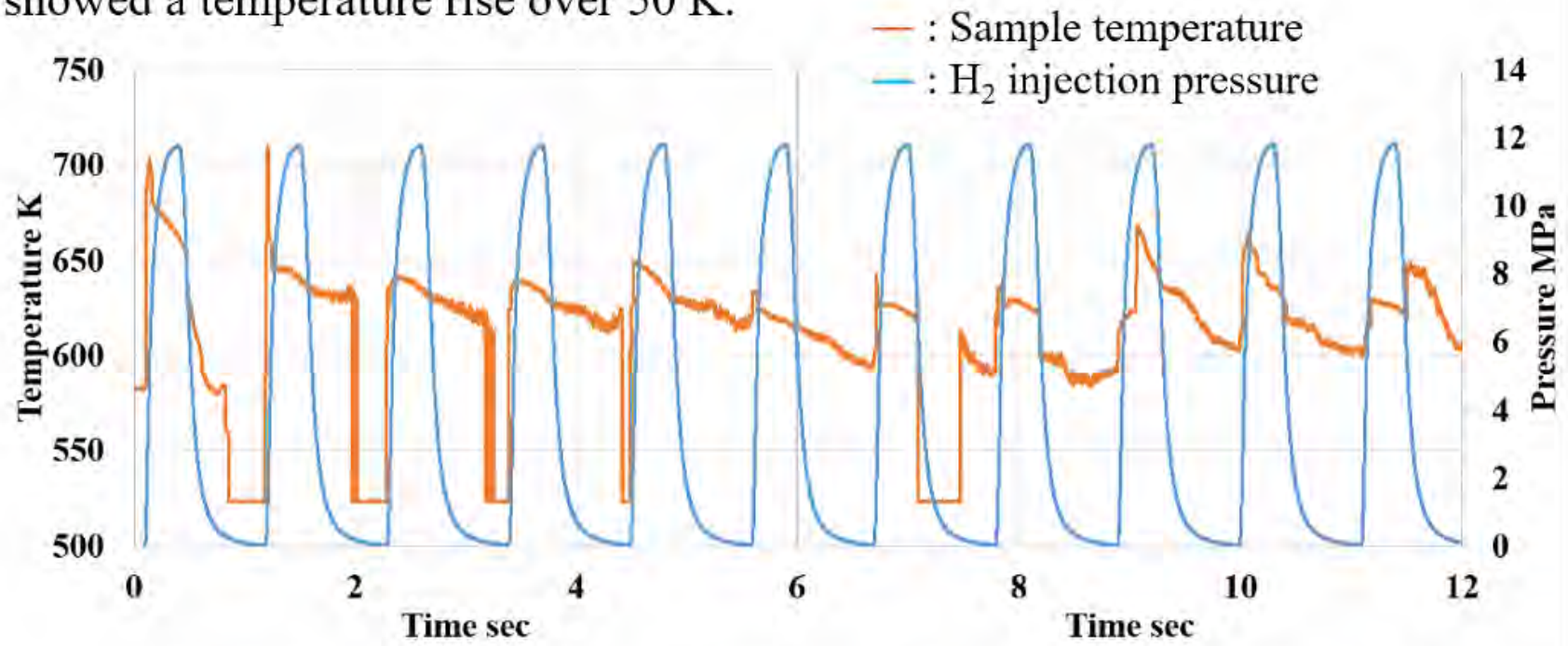


Fig 8. Results of the Continual Pulsed Injection Experiment using CNZ (11 Injections from the first injection)

RESEARCH QUESTION

Can a hydrogen-loaded Ni–Pd lattice produce a correlated signature of a non-conventional nuclear process?

HYLENR
TINY MATTERS

Background

Hydrogen-loaded metal systems have been reported to exhibit unusual combinations of:

- **Excess thermal output**
- **Helium / noble-gas formation**
- **Localized elemental and morphological changes**
- **Little or no detectable high-energy radiation**

The significance is not any one observation individually, but whether **multiple independent signatures occur together under controlled conditions**.

01 ENERGY	02 REACTION PRODUCTS	03 NUCLEAR EMISSIONS	04 MATERIAL RESPONSE
Thermometry + FLIR Thermal camera	Residual Gas Analysis	GM + Neutron Globe	SEM + EDX
Is there thermal output beyond the control response?	Are unexpected noble gases present?	Is conventional ionizing radiation produced?	Does the catalyst change locally / globally after operation?

Phase-1 Objective

Determine whether these four independent observables converge on a common experimental anomaly in BRT-NiUCS-2.

BRT-NiUCS-2 Reactor Configuration & Operating Conditions

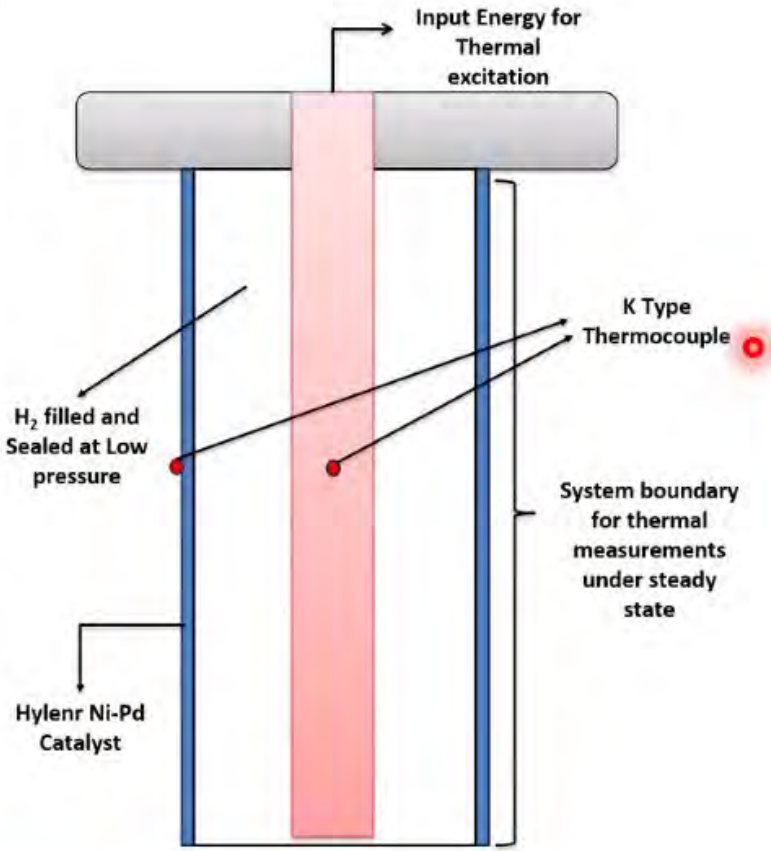
HYLENR
TINY. MATTERS.

ACTIVE REACTOR

- Proprietary Ni–Pd catalyst
- UHP hydrogen loaded
- Vacuum-sealed chamber
- Resistive internal heater
- Internal K-type thermocouple
- Heat-transfer-surface thermocouple
- Nominal electrical input: ~100 W

CALIBRATION REACTOR

- Same basic reactor architecture
- No active Ni–Pd catalytic mesh
- Argon substituted for hydrogen
- Comparable nominal gas pressure
- Same nominal electrical input (~100 W)



TEST PERIOD

Texas A&M monitored operation
27 Mar – 1 Apr 2026

OPERATING HISTORY

Cumulative operation
~30 days at ~100 W

Ni–Pd catalytic material ≈ 0.002% of total device mass

Phase-1 control difference: catalyst presence + H_2 vs Ar gas

METHODS

Measurement Methods & Instrumentation

HYLENR
TINY. MATTERS.

Each diagnostic probes a different part of the experimental signature.

01 THERMOMETRY

- K-type thermocouples at reactor core and heat-transfer surface
- FLIR infrared thermal imaging
- Cooling profiles following power-off

02 NUCLEAR DIAGNOSTICS

- Geiger–Müller counter: γ/X-ray
- He-3 neutron globe: neutrons
- ~5 days continuous monitoring
- Detector distance: ~1 m

03 RESIDUAL GAS ANALYSIS

- SRS RGA-100
- Faraday cup + CEM
- Mass scan: **m/z 1–100**
- Primary masses investigated:
  - m/z 4 — He-associated
  - m/z 20 — Ne-associated
  - m/z 40 — Ar-associated
  - m/z — Kr-associated
  - m/z 28 — atmospheric-leak indicator

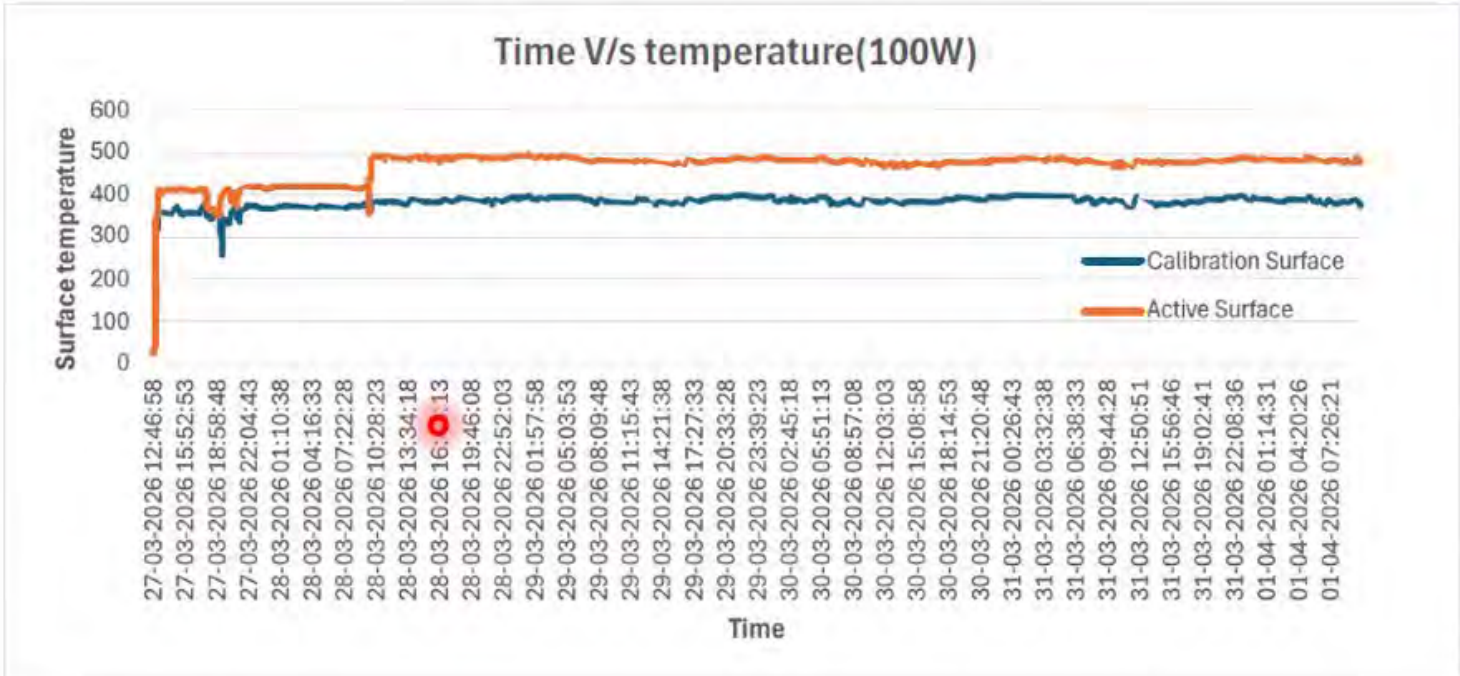
04 POST-REACTION CHARACTERIZATION

- Tescan LYRA-3 FIB/SEM
- SEM: morphology
- EDX: elemental distribution + relative concentration
- Pre-reaction material as reference

The Active Reactor Maintained Steady State Thermal Separation

HYLENR
TINY. MATTERS.

Comparison performed at steady state under comparable nominal ~100 W electrical input.



OBSERVATION

Active reactor maintained a higher heat-transfer-surface temperature than the control/calibration reactor.

STEADY-STATE SEPARATION

Peak sustained surface-temperature difference observed: ~100 °C

INTERPRETATION

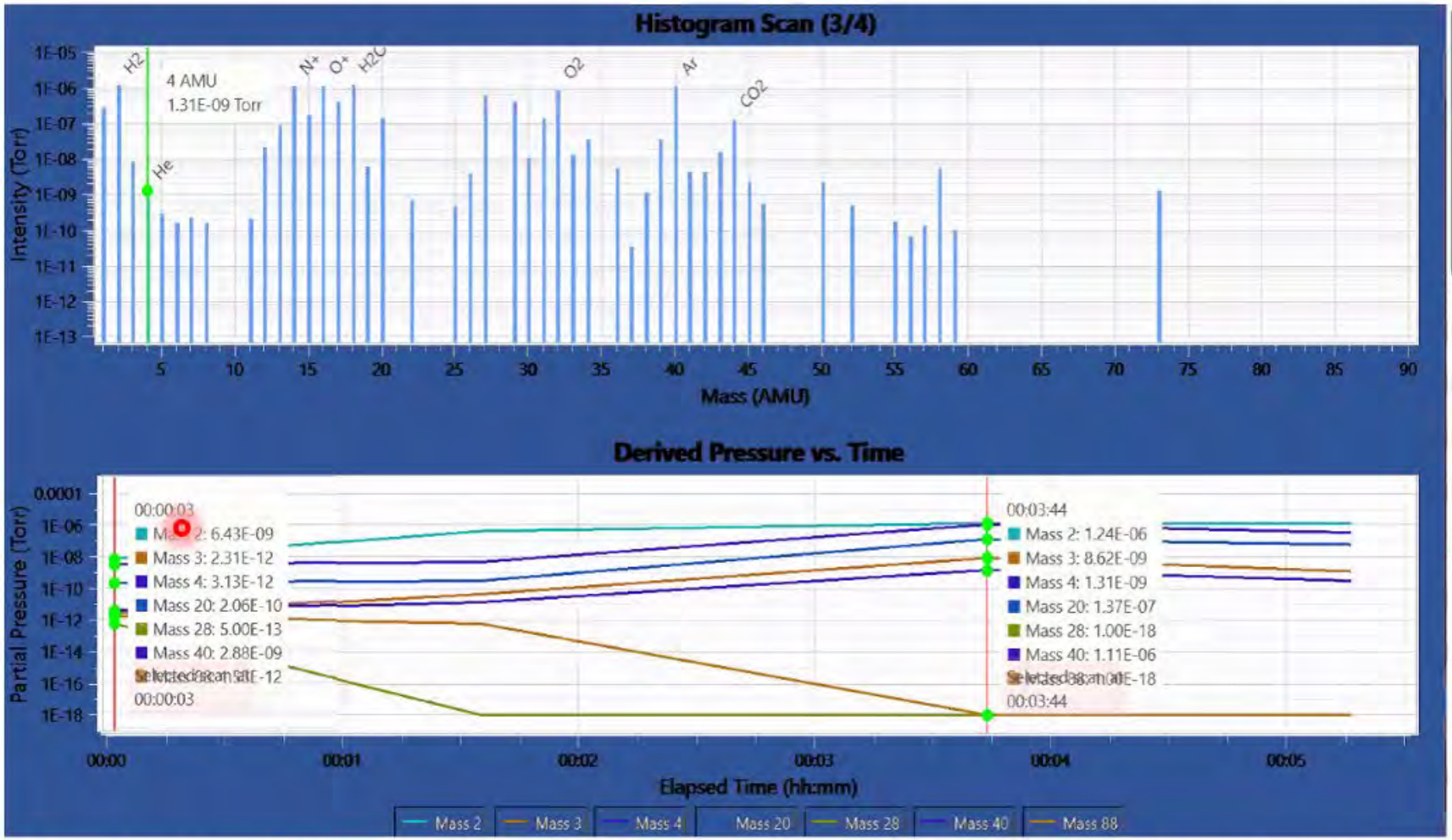
Persistent active/calibration thermal differential under comparable nominal input.

Boundary condition: both devices ~1.3 kg, similar atmospheric heat sink; thermocouple + FLIR behavior consistent.

Phase-1 limitation: comparative thermometry; dedicated calorimetry is required for quantitative excess-power determination for energy balance

He-, Ne- and Ar-Associated Signals Increased Without a Corresponding Nitrogen Increase

Reported noble-gas-associated signals rose by roughly 2–3 orders of magnitude relative to background-qualitative



m/z 4
He-associated
↑
~2–3 orders

m/z 20
Ne-associated
↑
elevated

m/z 40
Ar-associated
↑
~2–3 orders

m/z 28
N_2-associated
↔ / ↓
no corresponding rise

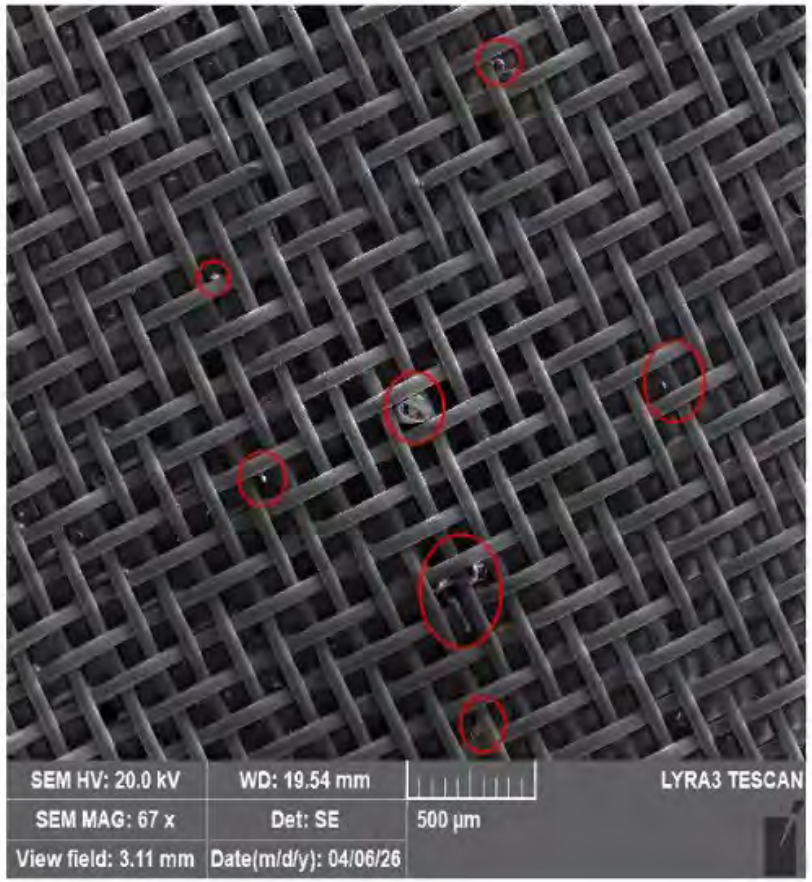
Atmospheric-leak check

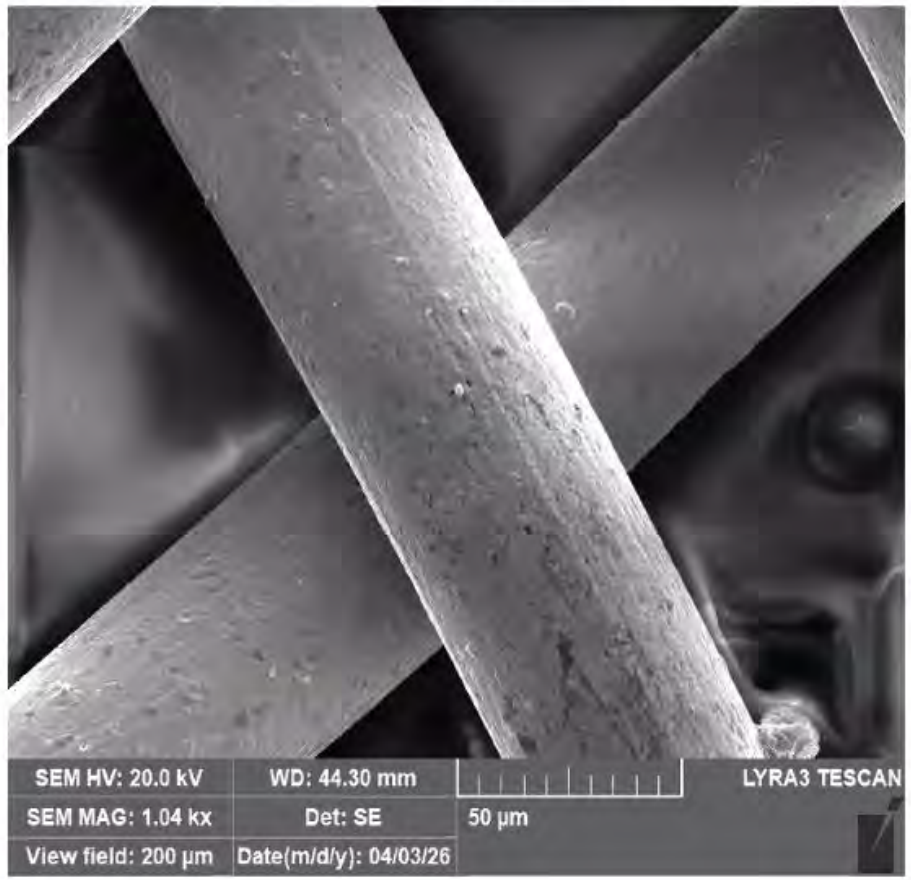
No corresponding increase in nitrogen partial pressure was observed.

Limitation: quadrupole RGA identifies mass-to-charge signals; isotope-resolved confirmation remains necessary for energy balance

Post-Reaction Catalyst Develops Localized Eruptions and Outgrowths

The changes are spatially localized rather than uniform across the catalyst mesh.





Observations

- Eruption-like structures
- Connected outgrowths
- String-like features
- Film like features
- Selected ordered structures- with toroidal geometry
- Cloud like , wavey surface morphology

Control comparison

Comparable features were absent from the pre-reaction same-batch reference.

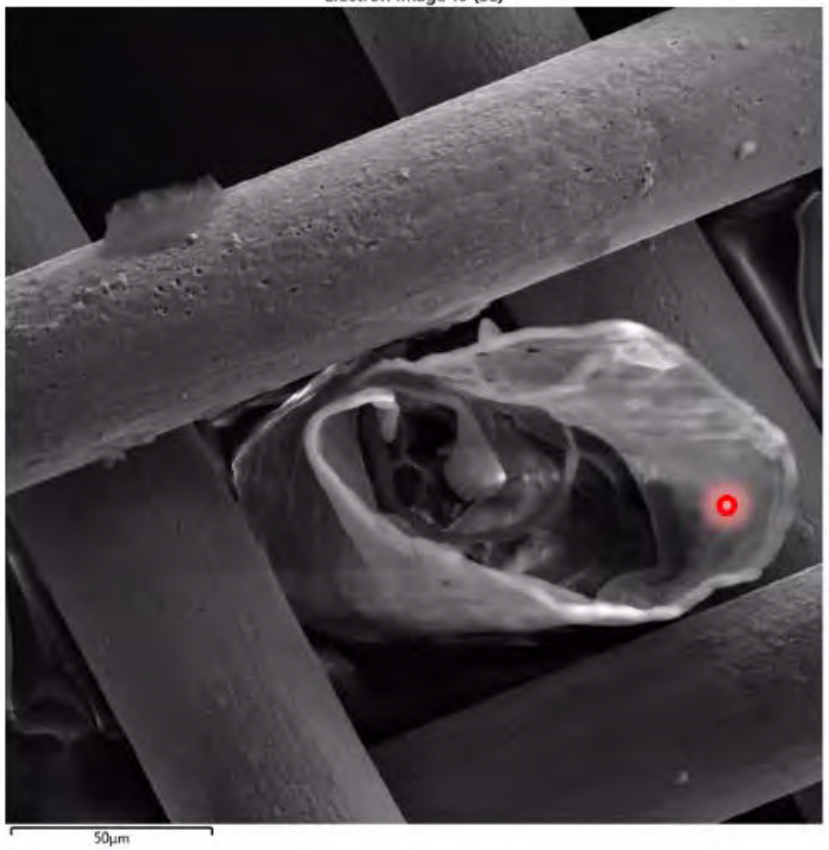
Why do the material modifications occur at discrete catalyst sites rather than uniformly across the heated mesh?

Post-Reaction Structure showing strings and film like features

Electron Image 9 (SE)



Electron Image 10 (SE)



Electron Image 7 (SE)

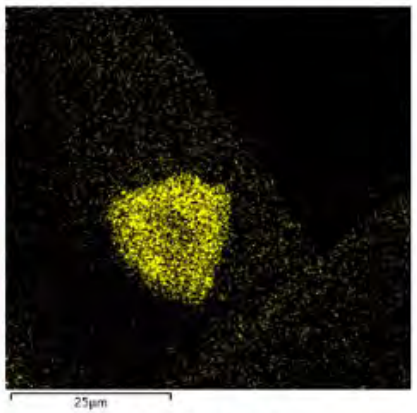


Localized Ca–C-Rich Region: Stoichiometric Interpretation Under Investigation

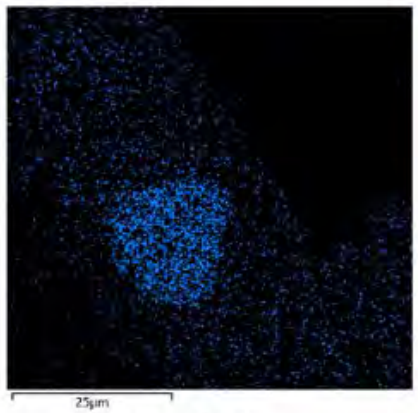
EDX demonstrates elemental co-localization; it does not by itself establish a specific CaC_3 phase.



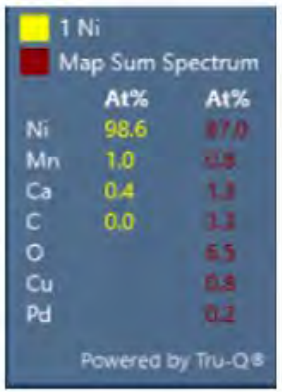
EDS Map

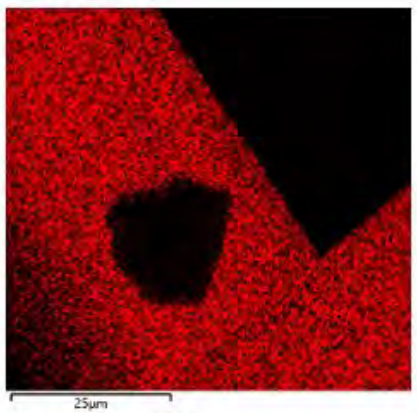


C Kα1,2

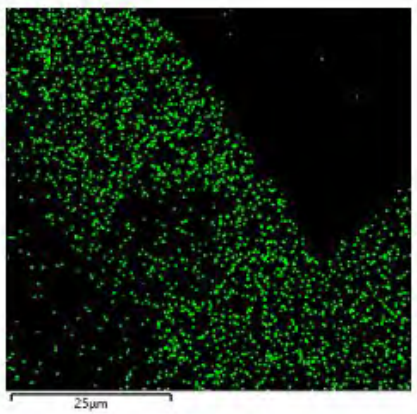


Ca Kα1

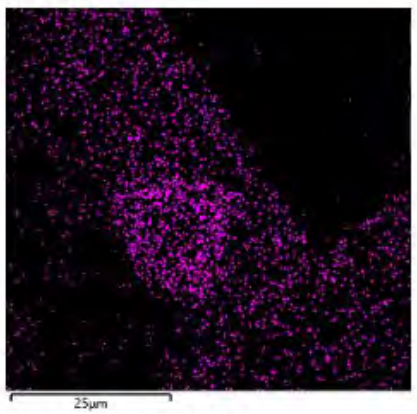




Ni Kα1



Pd Lα1



O Kα1

WHAT THIS SUPPORTS

A compositionally distinct Ca–C-O rich region within the abnormal feature without Ni

Next confirmation: FIB cross-section + localized EDX spectrum + phase-sensitive analysis (e.g., TEM/SAED, XRD/Raman as appropriate).

FUTURE WORK

Future Work I: Resolve the Eruption From Surface to Subsurface — and Element to Isotope

The next step is to determine where the structures originate and whether their elemental/isotopic composition differs from the starting material.

FIB CROSS-SECTION THROUGH REPRESENTATIVE ERUPTIONS

- Identify representative eruption / ordered structure
- Mill a FIB trench through the site
- Cross-sectional SEM/EDX through eruption + substrate
- Determine whether a void / defect-rich region sits beneath the feature
- Track Ni depletion, Fe-rich core and elemental layering through depth
- Distinguish surface deposition from subsurface nucleation

ISOTOPE-RESOLVED ANALYSIS

Noble gases
- ^{3}He / ^{4}He
- Ne isotope ratios
- Ar isotope ratios

Solid material
- SIMS / ICP-MS as appropriate
- Compare untreated material, normal post-reaction substrate, eruption and ordered / Fe-core structure

Reconfirm High AMU Elements – Ta , Yb , Ho through Mass spectrometry

Decisive question: do anomalous sites contain depth-resolved structures or isotope ratios inconsistent with the starting material, known contaminants and natural-abundance pathways?



Studying the Scaling Laws in a Plasma Reverse Vortex Reactor (PRVR). LENR Regime

Presented by:
Anatoly Klimov,
Sergey Altunin

Klimov.anatoly@gmail.com

ICCF27, Niagara Falls, Canada

With the support of ENG8,
patents applied for March 2026

ENG8
CLEAN ABUNDANT ENERGY

Objective of This Work

1. One of the most **important problems** of a low energy nuclear reaction physics **(LENR)** is the study of

   the Law of Similarity and Scaling of Extra Energy Release

   in any type LENR reactor depending on the *volume of the reaction zone* (for example, in a plasma vortex reactor PVR).

2. This issue was discussed at the **International Conference IWAHLM16** in Strasbourg,2025 and **IWAHLM17** in Bergamo, Italy, 2026, **[1]**
3. The present work is devoted to the consideration of this Task.

---

[1] Jacques Ruer, Jean-Paul Bibérian, et.all., A LENR Based Reactor, IWAHLM-17 Abstracts of Oral Presentation, P.25

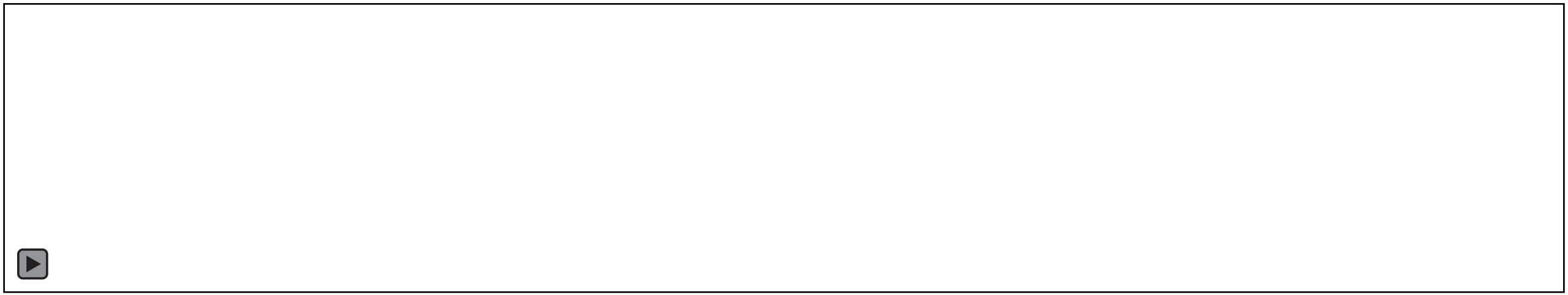
Heterogeneous Plasmoid Created by Pulsed Repetitive Electric Discharge in Swirl Flow in PVR-D

High-speed video.

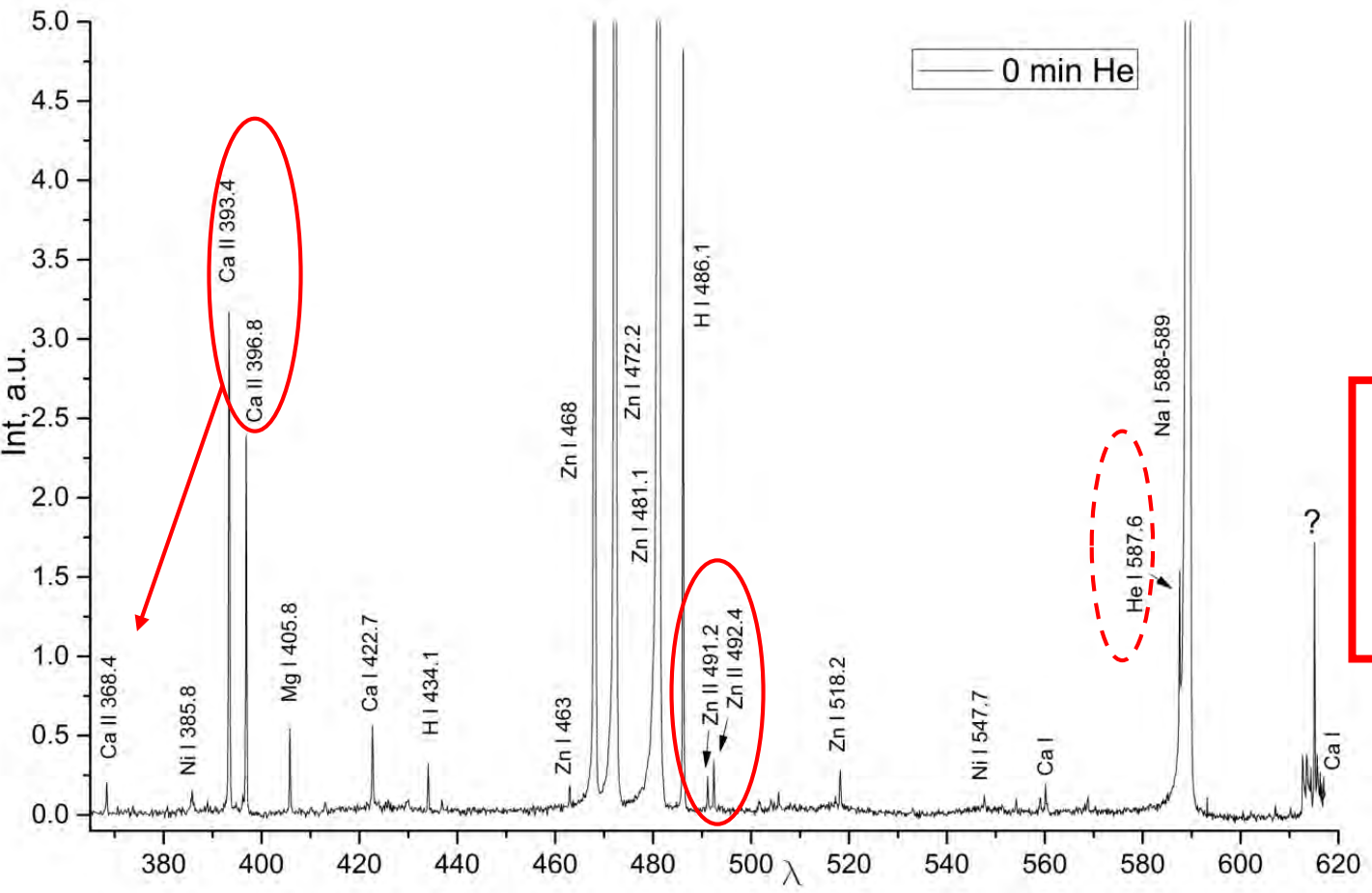
F_{exp}=10000 Hz, t_{exp}=100 μs

Gas mixture Ar : H20 = 10 : 1.

Axial velocity Vx is closed tangential velocity Vt: Vx~ Vt ~ 30 m/s, Pst ~ 1.5 bar.



Anode **Cathode**



What is the **powerful energy source** of creation for the highly excited transmuted ions ***(ZnII, CaII and others)?***

Excitation energy of these ions E=10-100 eV*
Plasma electron energy T_e=0.7 eV

*Direct confirmation of **LENR** in a PRVR:*

$$Ni_{28} + H_1 \longrightarrow Cu^*_{29}$$
$$Cu_{29} + H_1 \longrightarrow Zn^*_{30}$$

The typical optical spectrum of a heterogeneous plasma in a testing gas flow mixture: air + water steam = 94: 4: 2. **PRVR**

PRVR's HIGHLIGHTS, [1]

1. The maximum measured continuous X-ray radiation was located in the quantum energy range **E~ 1-10 keV.**

2. It was shown that there is the transformation of initial chemical elements with the creation of new transmuted elements such as ***C, Al, Na, K, Si, Ca, Zn*** in the output heterogeneous plasma (HP) flow (using pure *Nickel* electrodes, **99.99%+** Water steam).

3. Optical lines of strongly excited and multiple charged ions of the following ***elements Li II, CII, Al II, CaII, Cu II, and Zn II*** with an excitation energy of **10-100 eV** were recorded in the optical spectra of HP. Note that the measured electron temperature **T_e** of this HP was about **T_e~1 eV** only.

   Question: *- What is the energy source of creation f*

   or the highly excited levels of the listed ions? !!!!

4. Based on the **items 1 - 3**, it is possible to make an assumption about the implementation of LENR in heterogeneous plasma in PRVR.

*[1] Klimov A., Two-Stage LENR Plasmoid Vortex Reactor, IWAHLM-17 Abstracts of Oral Presentation, P.25

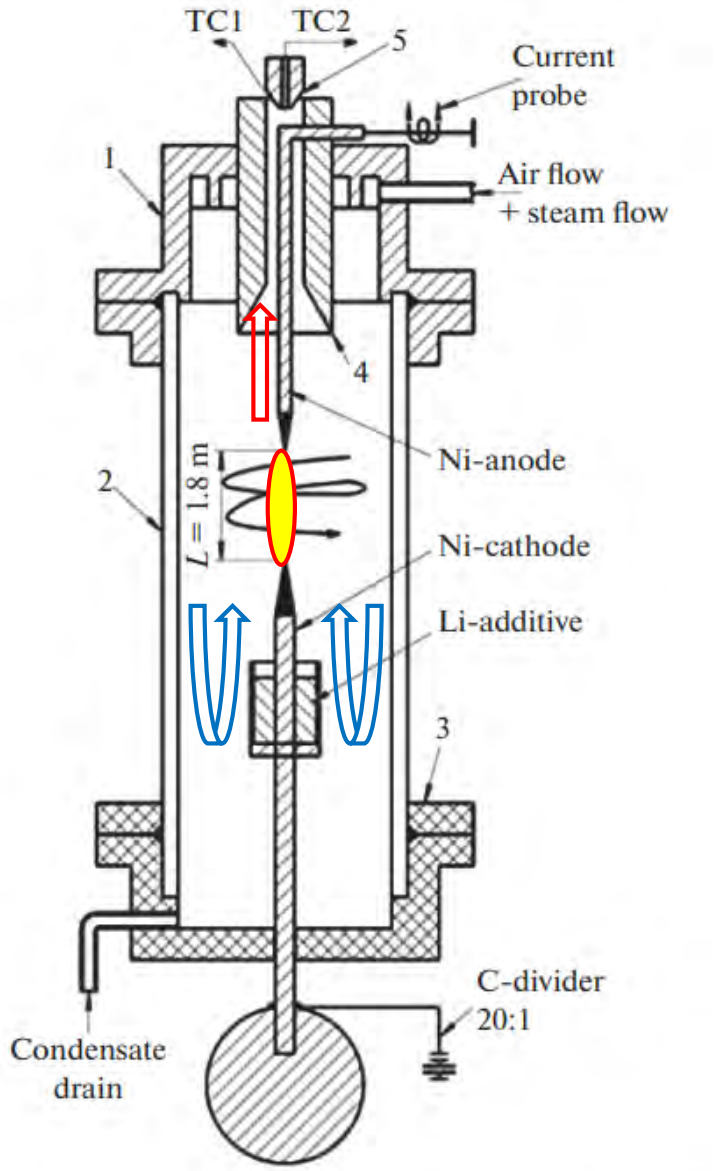
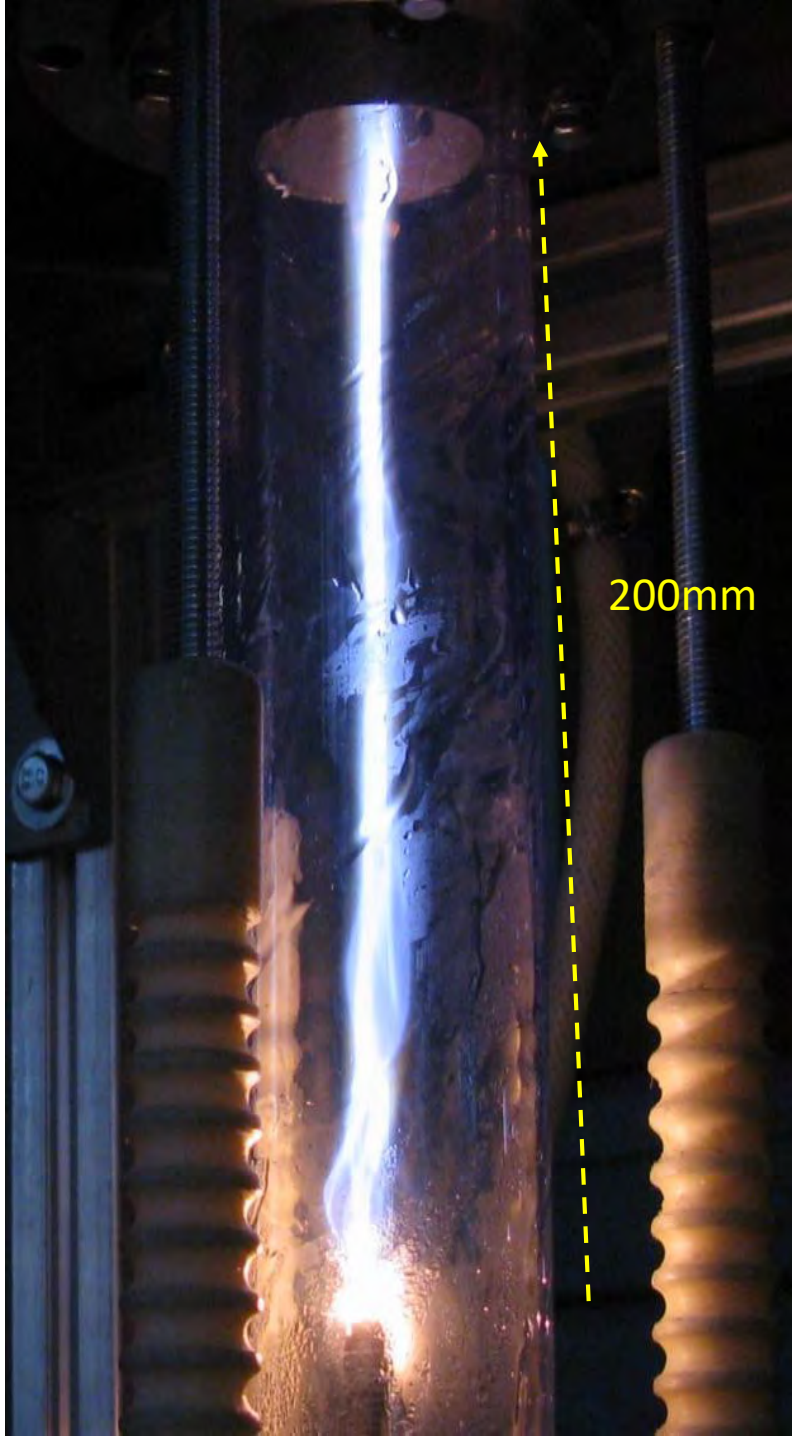


Fig. 1. The scheme of the reverse-vortex PVR for creating an extended RF plasma. The numbers indicate: 1—swirler (vortex generator), 2—quartz glass working section, 3—~~fan~~, 4—outlet nozzle, 5—shut-off cone with measuring thermocouples TC1 and TC2.



Experimental Setup Plasma Reverse Vortex Reactor (PRVR) used in this work

2026

left

Longitudinal HF plasmoid up to 40- 400 mm length in the PRVR

right

Plasma *Reverse* Vortex Reactor (PRVR). What is it???

Advantages PRVR comparing with direct swirl flow **PVR-D :**

- Possibility to create a longitudinal heterogeneous plasmoid **up to 1 m length** by HF discharge (capacity type) at atmospheric static pressure
- **Effective mixing** ⟹ *For example:* water steam flow + airflow
- Possibility to use **lean mixtures**. *For example:* water steam + airflow~ (**4 : 96)%**
- **Very stable LENR in a lean mixture regime**.
- **Small size**
- Optimal **wall and electrode cooling** and thermal energy protection

Summary

Scaling law of LENR in swirl plasma flow is best studied in **PRVR**

“Road Map” of a Calorimetric Experiment in the PRVR

- *Step #1*

Calibration experiment. Measuring of thermal losses in PRVR *by electric heater.* Estimation of heat loss coefficient **K_h**

- *Step#2*

Calorimetric experiment without the estimation of PRVR’s heat losses (**K_h**). **COP_x**

- *Step #3*

Calorimetric experiment with estimation of a total value **COP_0** in PRVR using heat loss coefficient, **K_h**.

Calibration Experiment. Step 1

1. Calibration experiment to determine heat losses in the PRVR reactor were carried out in **pure argon flow (1)** heated by HF plasma as well as in testing gas mixture heated by **electric heater (2),** [1].

2. The value of heat losses **K_h** in the PRVR is determined by the following formula

$$K_h = Q_{Ar} / N_e \quad (1)$$

where $Q_{Ar} = C_{p,Ar(T)} M_{Ar} (T_{out} - T_{in}) C_{p,Ar}$ - heat capacity of argon, M_{Ar} mass argon flow rate, N_e - input electric power in plasma

---

[1] Klimov A., Russian Journal of Physical Chemistry B, 2026, Vol. 20, No. 5, pp. 555–560

The Methodology of Performing a Calorimetric Experiment. Step 2

1. In this reactor PRVR, the value of a creation of *output thermal energy effectiveness* COP_x is calculated using the following formula:

$$\mathbf{COP_x = Q_T^*/N_e \ (2).}$$

where N_e - input electric power in plasma; $\mathbf{Q_T^*}$- output thermal power

2. Taking into account the measured heat losses $\mathbf{K_h}$ in this reactor one can obtain the total value $\mathbf{COP_o}$:

$$\mathbf{COP_o = Q_T^*/N_e K_h \ (3).}$$

---

3. When calculating the value of COP_s from the “electric socket", instead of N_e in the formulas, the value of N_{es} measured by the power meter is used

- $\mathbf{COP_{x,e} = Q_T^*/N_{es} \ (4).}$

4. Taking into account heat losses:

- $\mathbf{COP_{o,e} = Q_T^* N_{es} /K_h \ (5).}$

PRVR Calibration in Argon Flow.

Protocol #1

- Mass argon flow rate — M_{Ar} = 1.6 G/s
- Output argon flow temperature — T_{in} = 10C
- Output argon flow temperature — T_{out}= 95C
- Thermal power of the argon flow — Q_{Ar} = 68 W
- Input electric power — N_e~ 100 W
- Heat losses 1 — **K_{h1} = ~ 0.7 at L=50mm**
- Heat losses 2 — **(K_{h2} = ~ 0.5 at L=120mm)**

where

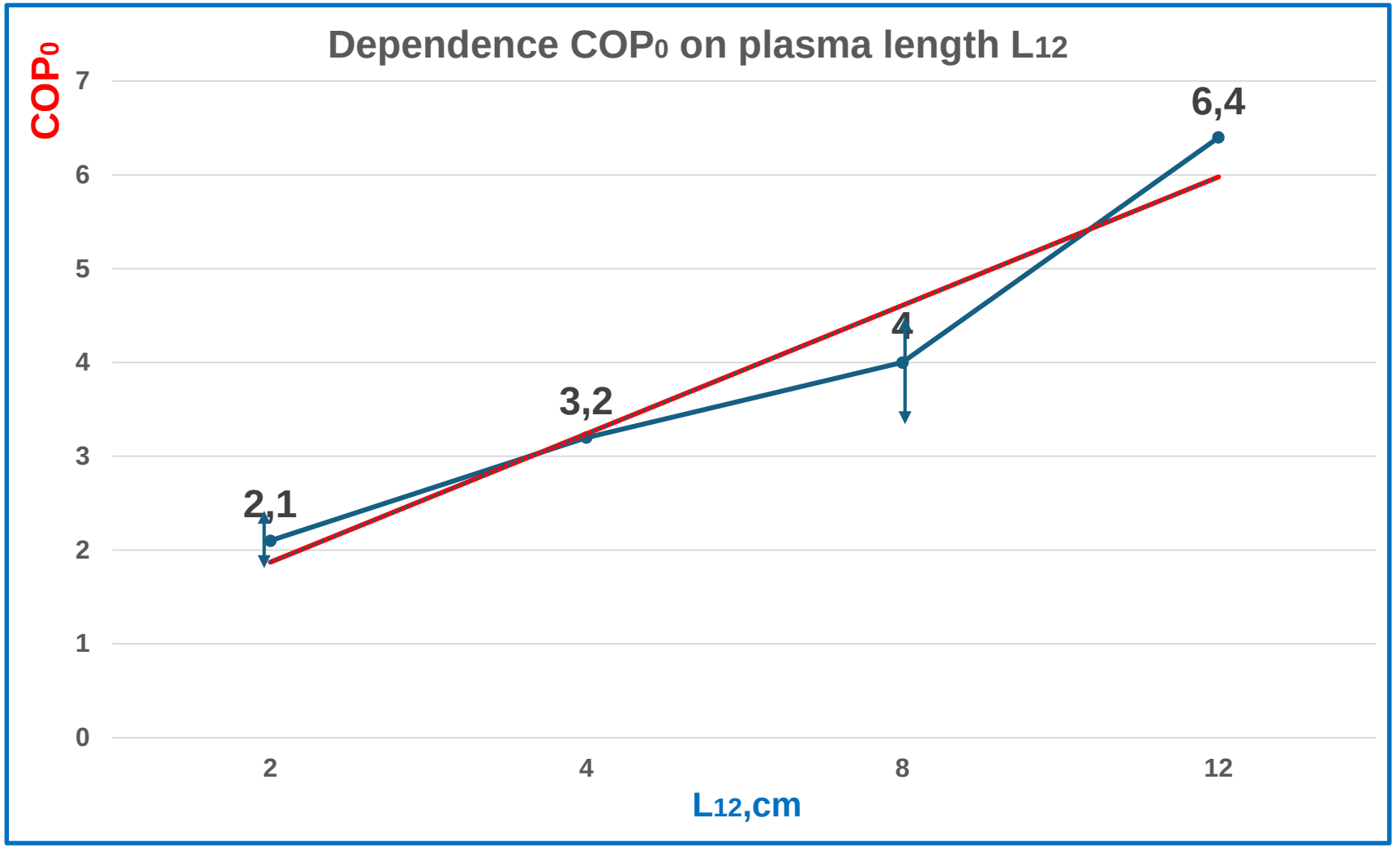
- $\mathbf{Q_{Ar} = C_{p,Ar(T)} M_{Ar} (T_{out} - T_{in})}$, where $\mathbf{C_{p,\,Ar}}$ - heat capacity of argon
- **$K_h = Q_{Ar} / N_e$**

Main Experimental Results. Small HF Plasmoid

Typical Protocol #2

- Electrodes — Nickel, 99,99%, diameter 6mm
- Distance between electrodes - **50 mm**
- Testing gas - Air flow+ water steam = (96 : 4)%
- Air mass flow rate - **M_{air} = 18,75 G/s**
- Water steam mass rate **M_{H2O}= 0,8 G/s**
- Input airflow temperature- **T_{in}= 60.7C**
- Output airflow temperature - **T_{out}= 183C**
- Output airflow thermal power- **Q_{air} = 2287 W**
- Input electric power - **N_e = 1060 W**
- **COP_0** = COP_x / K_h — **3,1** at K_h = 0.7

Summary Experimental Results in PRVR



Practical Results with ENG8 – Industrial Methane Burner Replacement

Roller-kiln gas burners at a 6MW SACMI line that ENG8 is in the process of replacing. Each burner is 50 kW-rated; the EnergiCell is sized to the rating, not the average duty. EnergiCell thermal generator system on test design output is 100kW.



Trials starting in Q4. Energy sales anticipated shortly after trials start.

Practical Results with ENG8 –

Domestic Natural Gas Replacement Now

Domestic and commercial space heaters. 5-10 kW-rated; Installation testing at a residential property in Portugal. Discussions starting regarding licencing with domestic, commercial and industrial HVAC and gas boiler manufacturers.

